



Coupled Monte Carlo and thermal-fluid modeling of high temperature gas reactors using Cardinal

A.J. Novak ^{a,*}, D. Andrs ^b, P. Shriwise ^a, J. Fang ^a, H. Yuan ^a, D. Shaver ^a, E. Merzari ^c, P.K. Romano ^a, R.C. Martineau ^a

^a Argonne National Laboratory, United States

^b Idaho National Laboratory, United States

^c Pennsylvania State University, United States



ARTICLE INFO

Article history:

Received 19 April 2022

Received in revised form 22 June 2022

Accepted 27 June 2022

Available online 22 July 2022

Keywords:

Cardinal

MOOSE

OpenMC

NekRS

Monte Carlo

CFD

ABSTRACT

Cardinal is an open-source application that couples OpenMC Monte Carlo transport and NekRS computational fluid dynamics to the Multiphysics Object-Oriented Simulation Environment (MOOSE), closing neutronics and thermal-fluid gaps in conducting high-resolution multiscale and multiphysics analyses of nuclear systems. We provide an introduction to Cardinal's software design, data mapping, and multiphysics coupling strategy to highlight our approach to overcoming common challenges in multiphysics simulation. We then describe an application of Cardinal to prismatic High Temperature Gas Reactors (HTGRs) with various combinations of NekRS, OpenMC, BISON, and THM. A high-resolution coupling of NekRS, OpenMC, and BISON provides a reference solution at the unit cell level and shows excellent agreement with a lower-resolution coupling of THM, OpenMC, and BISON. A full core coupling of THM, OpenMC, and BISON resolving the three-dimensional conjugate heat transfer and sub-pin power distribution then provides detailed predictions of HTGR temperatures and the fission distribution.

© 2022 Elsevier Ltd. All rights reserved.

1. Introduction

High Temperature Gas Reactors (HTGRs), of either the pebble or prismatic block variety, offer many attractive design features. The high-temperature compatibility of the helium coolant with conventional structural materials, combined with the high-temperature fission product retention of the TRISO fuel (Demkowicz et al., 2019), enables high-temperature operation and applications to the process heat sector. In addition, the helium primary loop may potentially be coupled to a Brayton cycle to achieve high efficiency (McDonald, 1990). A transparent and inert coolant reduces activation and, when pure, may exhibit simpler corrosion considerations than other high-temperature coolants such as molten salts (Graham, 1990; Zheng and Sridharan, 2018). The presence of large quantities of graphite also introduces high thermal inertia, slowing the propagation of thermal transients.

One challenge associated with the modeling of TRISO-fueled systems is the complex fuel structure. For the prismatic HTGR variety, a TRISO fuel matrix is formed into cylindrical compacts filling

hundreds of machined channels in hexagonal graphite blocks. In each block, additional machined channels provide coolant flow paths and accommodate poison or moderator pins. The full core is then composed of a lattice of these fuel blocks.

In pin-type reactors such as Light Water Reactors (LWRs), the fuel pins are thermally separated from one another by highly-turbulent fluid flow. For these systems, the turbulent fluid mixing allows 1.5-D conduction models to reasonably approximate the Conjugate Heat Transfer (CHT) physics while neglecting axial and azimuthal variations in temperature and power. Conversely, in prismatic HTGRs a graphite "webbing" interconnects the fuel compacts, coolant channels, and poison/moderator pins, resulting in highly multidimensional CHT. To reduce computational requirements, the thousands of HTGR fuel compacts are sometimes grouped into N "representative" pins that couple to a continuous graphite webbing, with nonlinearities resolved via Picard iteration. The strong coupling between the heat transfer and neutron transport physics, especially near reflector power peaks (Ma et al., 2021; Novak et al., 2022), may lead to numerical instabilities as the coupled physics domains become increasingly separated into distinct single-physics/"representative" domain models (Laboure et al., 2019).

A number of reactor designers are pursuing small modular or microreactors that use prismatic HTGR fuel concepts. In terms of

* Corresponding author at: Argonne National Laboratory, United States.

E-mail address: anovak@anl.gov (A.J. Novak).

the radiation transport physics, the smaller size of these systems may result in stronger boundary effects and reduced accuracy of diffusion methods. Together, these neutron transport and Thermal–Hydraulic (T/H) physics considerations suggest that reference reactor core simulations may benefit from 3-D, pin-resolved multi-physics couplings of CHT and Monte Carlo transport.

For small-size reactors, high-resolution tools may serve an important role in the nuclear design and licensing processes in areas such as 1) identifying sensitive closures/assumptions in lower-resolution models and re-calibrating where necessary; 2) verifying coarse-mesh tools; and 3) assessing differences between the “paper” reactor and the as-built design. Recognizing the importance of 3-D high-resolution tools to the design and analysis of prismatic HTGRs, the Nuclear Energy Advanced Modeling and Simulation (NEAMS) Center of Excellence (CoE) for Thermal Fluids Applications in Nuclear Energy initiated a project with the goal of applying the Cardinal multiphysics modeling tool to HTGRs.

Cardinal is an open-source Multiphysics Object-Oriented Simulation Environment (MOOSE) application that wraps the NekRS spectral element Computational Fluid Dynamics (CFD) code (Fischer et al., 2021) and the OpenMC Monte Carlo radiation transport code (Romano et al., 2015) within the MOOSE framework (Permann et al., 2020). Cardinal leverages MOOSE’s physics- and geometry-agnostic multi-application and data transfer systems to enable high-resolution multiphysics feedback coupling to other MOOSE tools. By adopting the plug-and-play philosophy of MOOSE, Cardinal has been applied to very diverse systems, including multiphysics coupling of NekRS, OpenMC, and BISON for a 7-pin Sodium Fast Reactor (SFR) (Novak et al., 2022) and a small salt-cooled Pebble Bed Reactor (PBR) with 1568 pebbles (Merzari et al., 2021); CHT coupling of NekRS and BISON for a salt-cooled PBR with 127000 pebbles (Fischer et al., 2021); separate and overlapping domain coupling of NekRS and SAM for systems-level analysis (Huxford et al., 2022); and coupling of NekRS and the MOOSE tensor mechanics module for pressurized thermal shock in reactor pressure vessels (Yu et al., 2022).

In this work, a multiphysics coupling of OpenMC, NekRS, the MOOSE Thermal Hydraulics Module (THM) (Berry et al., 2014), and BISON (Hales et al., 2016) is performed using Cardinal and applied to a generic prismatic HTGR at both the unit cell and full core level. The objectives of this work are threefold; the first goal is to demonstrate the usage of NEAMS tools for high-resolution multiphysics analyses of HTGRs. The second objective is to illustrate how the plug-and-play nature of MOOSE facilitates multiscale modeling, by allowing seamless interchange of T/H models of varying resolution. In this work, the coolant channels are modeled by either a NekRS Reynolds Averaged Navier Stokes (RANS) CFD model or a THM 1-D area-averaged Navier–Stokes model. Finally, the third objective is to develop publicly-available tutorials to assist users in adopting Cardinal. Tutorials for a unit cell and single assembly model of a HTGR are available on the Cardinal documentation website (CELS, 2022) and have also been added to the Virtual Test Bed repository (Feng et al., 2021).

It is important to emphasize that the objectives of the CoE project are to provide a “proof-of-concept” demonstration of Cardinal for HTGRs – not to model a specific, late-stage industry concept or conduct design studies. All results shown in this work should only be taken as indicative of Cardinal’s capabilities for prismatic HTGR analysis, with sufficient detail and complexity to be relevant to many other HTGR concepts. As such, all validation is left to future work.

The remainder of this paper is organized as follows. Section 2 introduces the computational tools used for analysis – OpenMC, NekRS, BISON, and THM – as well as how they are coupled together via Cardinal. In Section 3, the HTGR specifications are presented. Section 4 describes in detail the coupling strategy. In Section 5, Cardinal is then used to model the unit cell geometry using a

high-resolution coupling of OpenMC, NekRS, and BISON and a comparatively lower-resolution coupling of OpenMC, THM, and BISON. The NekRS-based model is used to develop a Nusselt number closure for THM and evaluate the impact of the thermal-fluid modeling choice on the coupled physics solution. After demonstrating good agreement between NekRS and THM, Section 6 presents a full-core coupling of OpenMC, THM, and BISON. Pin-resolved predictions are provided for the fission distribution, fluid temperature, and solid temperature. Finally, Section 7 revisits the limitations of the modeling and simulation, and outlines future work.

2. Computational tools

This section introduces each single-physics tool and describes the governing equations solved in the context of the present application. Then, Section 2.5 introduces Cardinal and describes how OpenMC and NekRS are coupled to MOOSE.

2.1. OpenMC

OpenMC is an open-source continuous-energy neutron-photon Monte Carlo code with capabilities for cell and libMesh unstructured mesh tallies, k -eigenvalue and fixed source calculations, event- and history-based parallelism, depletion, windowed multipole on-the-fly Doppler broadening, and many other features (Romano et al., 2015). In the present work, the OpenMC models are built using a Constructive Solid Geometry (CSG) cell-based representation of the geometry.¹ Woodcock delta tracking and mesh-based geometries are both currently under development in OpenMC, so temperatures and densities are uniform over an individual cell.

The fission distribution is measured with a kappa-fission tally, or the recoverable energy release from fission in units of eV/source. The TRISO particles are represented explicitly, with positions determined using Random Sequential Addition (RSA) to achieve the desired packing fraction. Finally, cross section data is provided with the ENDF/B-VII.1 library, which has data sets between 250 K and 2500 K. For the $S(\alpha, \beta)$ thermal scattering data and Unresolved Resonance Region (URR) probability tables, an in-memory stochastic linear-linear interpolation between the nearest two temperature data sets is performed, whereas the windowed multipole method is used for the resolved resonance range. Many previous researchers have explored the effect of the interpolation strategy on accuracy in either the microscopic cross sections themselves (Trumbull, 2006) or else on secondary parameters such as reaction rates (Seker et al., 2007; Vazquez et al., 2012; Ivanov et al., 2011). Future work may include sensitivity studies on the library temperature spacing for the $S(\alpha, \beta)$ and URR tables.

2.2. NekRS

NekRS is an open-source spectral element CFD code with capabilities for RANS modeling, Large Eddy Simulation (LES), and Direct Numerical Simulation (DNS) (Fischer et al., 2021). By using the Open Concurrent Compute Abstraction (OCCA) interface, NekRS supports both CPU and GPU backends. In the present work, NekRS solves for fluid mass, momentum, and energy conservation with an incompressible RANS model,

$$\nabla \cdot \vec{u} = 0 \quad (1)$$

$$\rho_f \left(\frac{\partial \vec{u}}{\partial t} + \vec{u} \cdot \nabla \vec{u} \right) = -\nabla P + \nabla \cdot (\mu_f + \mu_T) \nabla \vec{u} \quad (2)$$

¹ With the exception of the phrase “unit cell” (which is used to describe a geometrically-repeatable unit of the HTGR), any phrase with the word “cell” (such as “OpenMC cell” or “cell tally”) refers to a region of space in the Monte Carlo model.

$$\rho_f C_{pf} \left(\frac{\partial T_f}{\partial t} + \vec{u} \cdot \nabla T_f \right) = \nabla \cdot (k_f + k_T) \nabla T_f \quad (3)$$

where \vec{u} is the velocity, ρ_f is the density, P is the pressure, μ_f is the laminar dynamic viscosity, μ_T is the turbulent dynamic viscosity, C_{pf} is the isobaric specific heat capacity, T_f is the temperature, k_f is the laminar thermal conductivity, and k_T is the turbulent thermal conductivity. The turbulent Prandtl number Pr_T relates k_T and μ_T ,

$$Pr_T \equiv \frac{\mu_T C_{pf}}{k_T}, \quad (4)$$

which in the present work is selected as $Pr_T = 0.91$. The $k-\tau$ RANS model is then used to evaluate μ_T based on two additional Partial Differential Equations (PDEs) for the turbulent kinetic energy k and the inverse specific dissipation rate τ (Kok and Spekreijse, 2000; Thangam et al., 1991). Wall functions in NekRS are currently under development, so all NekRS models are wall-resolved such that $y^+ < 1$. All solution variables are represented as 7th order spectral element interpolations of Gauss-Lobatto-Legendre (GLL) quadrature points (Fichtner, 2011), giving $8^3 \equiv 512$ Degrees of Freedom (DOFs) per element. Because NekRS's $k-\tau$ model is currently limited to constant-property flows, ρ_f , μ_f , k_f , and C_{pf} are assumed constant at the inlet conditions.

2.3. THM

THM is an open-source MOOSE-based slope-reconstructed Discontinuous Galerkin (DG) thermal-fluids code applicable to single-phase systems-level analysis (Berry et al., 2014). Flow channels are represented as one-dimensional pipes with cross-sectional areas that vary along the length. THM solves for conservation of mass, momentum, and energy with area averages of the Navier-Stokes equations,

$$\frac{\partial}{\partial t} (A \rho_f) + \frac{\partial}{\partial x} (A \rho_f u) = 0, \quad (5)$$

$$\frac{\partial}{\partial t} (A \rho_f u) + \frac{\partial}{\partial x} (A \rho_f u^2 + AP) = \tilde{P} \frac{\partial A}{\partial x} - \frac{f}{2D_h} \rho_f u |u| A, \quad (6)$$

$$\frac{\partial}{\partial t} (A \rho_f E_f) + \frac{\partial}{\partial x} [Au(\rho_f E_f + P)] = H_w a_w (T_{wall} - T_{bulk}) A, \quad (7)$$

where x denotes the coordinate along the flow length, A is the channel cross-sectional area, $u \equiv \vec{u} \cdot \hat{n}_x$ is the x -component of velocity, \tilde{P} is the average pressure on the curve around the cross-sectional area, E_f is the total specific energy, f is the friction factor, D_h is the hydraulic diameter, H_w is the convective wall heat transfer coefficient, a_w is the heat transfer area density, T_{wall} is the wall temperature, and T_{bulk} is the bulk temperature. In the present work, f is given by the Churchill correlation (Churchill, 1977) and H_w is given by the Dittus-Boelter correlation (Berry et al., 2014).

Although NekRS requires an incompressible flow model, THM requires an Equation of State (EOS) that can provide the specific internal energy as a function of ρ_f and P . Therefore, THM uses the ideal gas EOS for density, with μ_f , k_f , and C_{pf} set to constant values based on the inlet conditions.

2.4. BISON

BISON is a MOOSE-based fuel performance code applicable to a wide variety of nuclear fuels (Hales et al., 2016). This work solves the steady state heat conduction equation for solid temperature T_s ,

$$-\nabla \cdot (k_s \nabla T_s) = \dot{q}_s, \quad (8)$$

where \dot{q}_s is the volumetric heat source. In order to have a fully open-source model, the actual heat conduction simulations are conducted with MOOSE's heat conduction module (which BISON uses internally for heat conduction). For brevity, "BISON" will be used in order to convey the heat conduction solver. In other words, the BISON executable can be used to run the models developed for this paper, but in order to release inputs as open-source tutorials, the actual solves are conducted with the MOOSE heat conduction module (which provides the same physics kernels as BISON).

It is currently impractical to resolve the trillions of TRISO particles in a full-core HTGR heat conduction solve. Most previous applications that do resolve TRISO particles have emphasized a partial compact (Kamalpour et al., 2018; Zhang et al., 2021; Weng et al., 2021) or a single pebble (Novak et al., 2021), geometries that are typically 4–6 orders of magnitude smaller than the full core geometry. The present application homogenizes the TRISO particles into the compacts by volume-averaging the thermal properties and heat source. By homogenizing the thermal resistance of the low-conductivity buffer layer, this process tends to underpredict fuel kernel temperatures (Novak, 2020). A more accurate approach is to instead employ multiscale techniques (Novak et al., 2021; Stainsby et al., 2009) that account for the thermal resistance of the TRISO layers and the "locality" of heat generation without explicitly resolving particles. Due to the plug-and-play design of MOOSE, future extensions of the present model can improve fidelity by incorporating the Heat Source Decomposition (HSD) multiscale model in the Pronghorn porous media MOOSE application (Novak et al., 2021).

2.5. Cardinal

MOOSE was initially developed for solving coupled systems of nonlinear PDEs (Permann et al., 2020). To utilize MOOSE in this manner, applied math practitioners can create C++ objects in an object-oriented framework to represent the physics kernels, Boundary Conditions (BCs), material properties, executioners, and any other aspects of the governing equations and solution strategy. MOOSE then coordinates libMesh and PETSc to discretize space using the Finite Element Method (FEM) and solve the nonlinear system. Many such "native" MOOSE applications have been developed, spanning domains including nuclear reactor physics, fluid flow, microstructure evolution, geothermal science, and advanced manufacturing.

The MultiApp system in MOOSE allows different MOOSE applications to be coupled together in a hierarchical tree with arbitrary depth. All MOOSE-based simulations have a single "main" application, which sits at the top of the coupling tree, underneath which may be an arbitrary number of nested "multiapps." Each multiapp may in turn control an arbitrary number of doubly-nested multiapps, and so on. Data is transferred vertically between applications via MOOSE's Transfer system, which provides physics-agnostic communication using mesh interpolations, nearest node lookups, mesh evaluations, copies, scalar and vector postprocessors, and many other means. The MOOSE Transfer system also facilitates transfers between applications operating with different dimensions, such as between 3-D and 1-D domains. The coupling tree is highly parallelized; the main application uses all processes, and all nested applications run simultaneously in parallel with the resources allocated to the local "parent" application.

In recent years, MOOSE has added the capability for coupled solves with "external" applications that are based on entirely different solution methodologies and software stacks. An external code can be "wrapped" into a MOOSE application by overriding a few key interface functions in MOOSE's ExternalProblem class. These interfaces initialize, run, and postprocess results for the external code, while exposing the time stepping, synchronization, and data transfer systems in MOOSE. These "MOOSE-wrapped

codes" are themselves MOOSE applications, but with physics engines substituted with Application Programming Interface (API) calls to the external code base. Such applications are also referred to as "non-native" MOOSE applications, because all aspects of the simulation are pulled from external libraries.

Cardinal is a non-native MOOSE application that wraps OpenMC and NekRS within MOOSE, allowing the radiation transport and CFD physics engines in OpenMC and NekRS to interact with the MOOSE framework. Fig. 1 depicts the overall relationship of Cardinal to the MOOSE framework and other native applications. The data transfers between applications (heat flux, power, temperature, etc.) are customizable and are dependent on the particular system being modeled. These data transfers are discussed in Sections 2.6 and 2.7.

There are three main steps to wrap OpenMC and NekRS within Cardinal. At a high level, Cardinal is responsible for:

1. Copying the mesh/geometry of the external application into the `MoosMesh` format. This mesh *mirror* is the receiving point for all field data sent in/out of the external code.
2. Establishing a spatial mapping from the external application's geometry to the `MoosMesh`.
3. Running the external application:
 - (a) Read data from `MooseVariable(s)` defined on the mirror and write into the source term/material property/BC data structures in the external application.
 - (b) Run the external application. For OpenMC, this calls `openmc::openmc_run` to run a k -eigenvalue calculation, whereas for NekRS this calls `nekrs::runStep` to run a single time step.
 - (c) Read data from the source term/material property/BC data structures of the external application and write into `MooseVariable(s)` defined on the mirror.

Cardinal essentially translates the NekRS and OpenMC solutions into a MOOSE-compatible format (i.e., the `MoosMesh`), allowing NekRS and OpenMC to be coupled to *any* MOOSE application – agnostic of the fact that the actual physics solve is performed by an external code. A purposefully general design allows NekRS and OpenMC to be coupled to *any* other MOOSE application in a plug-and-play manner, a structure that is sometimes referred to as "platform coupling." For instance, the same OpenMC model can provide neutronics feedback to NekRS turbulence-resolved CFD, Pronghorn subchannel/porous media models, and SAM 1-D flow loop models (Fischer et al., 2021; Novak et al., 2020; Hu, 2017). In a similar fashion, the same NekRS model can provide CFD feedback to a MOOSE tensor mechanics model, BISON fuel performance, Griffin deterministic neutronics, and OpenMC radiation transport (Hales et al., 2016; Romano et al., 2015).

Cardinal's design eliminates many limitations common to earlier T/H and Monte Carlo couplings. All data is communicated in-memory, obviating the need for code-specific I/O programs (Ivanov et al., 2013; Zhang et al., 2021; Mylonakis et al., 2017) and reducing file-based communication bottlenecks (Guo et al., 2017). In addition, mappings between the NekRS and OpenMC geometries to MOOSE are constructed automatically, with no requirements on node/element/cell alignment. This eliminates the need for rigid one-to-one mappings (Gurecky and Schneider, 2016) or careful attention to cell volumes (Romano et al., 2020), but more importantly, allows for geometry-agnostic data transfers. Cardinal's diverse applications to PBRs, SFRs, LWRs, and HTGRs are all conducted without the need to develop any custom source code or file I/O manipulation scripts.

The input files required to run a simulation consist of 1) the standalone code input files that would be needed to run individual OpenMC and NekRS simulations, and 2) a thin Cardinal input file that integrates the external codes into MOOSE. Different from

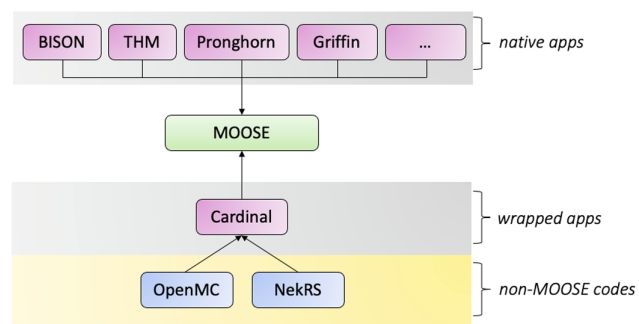


Fig. 1. Overall relationship of Cardinal to the MOOSE framework. All pink boxes are MOOSE applications.

other multiphysics coupling works (Liu et al., 2017; Yexin et al., 2017), the NekRS and OpenMC input files can identically be run as standalone cases (with NekRS and OpenMC executables) or through Cardinal (with a Cardinal executable). That is, there are no special "tags" in the NekRS and OpenMC input files indicating where/how to apply physics feedback, or any preordained/user-supplied geometry mapping information. Extensive documentation on the build system, input file syntax, and model setup can be found on the Cardinal website (CELS, 2022).

Cardinal is developed for High Performance Computing (HPC) deployment, and supports distributed mesh data transfers between NekRS, OpenMC, and MOOSE. Both MOOSE and NekRS may distribute the mesh and solutions among MPI ranks, reducing memory associated for transfers. OpenMC replicates the geometry across all ranks, but may still communicate with a domain-decomposed MOOSE solve. In addition, NekRS supports both CPU and GPU backends. When GPUs are available, Cardinal facilitates data transfers between the host (where MOOSE and OpenMC run) and device (where NekRS runs).

Sections 2.6 and 2.7 next describe Cardinal's NekRS and OpenMC wrappings in greater detail. An in-depth description of the Picard coupling strategy is then presented in Section 4.

2.6. The NekRS wrapping

Cardinal includes two modes for coupling NekRS to MOOSE – 1) boundary CHT coupling via temperature and heat flux wall BCs, and 2) volume coupling via volumetric heat sources, temperatures, and densities. In this work, we combine both modes together, such that NekRS communicates via CHT with BISON, but via densities and temperatures with OpenMC. Fig. 2 shows an example of the various mesh mirrors constructed by Cardinal for a NekRS pipe simulation coupled to a generic MOOSE application.

NekRS solves the Navier–Stokes equations on the "NekRS mesh" in the right-most pane, a high-order (i.e., 7th order) hexahedral mesh. The two options for mesh mirrors are shown in the middle pane; recall that the mesh mirrors are only used to receive field data for coupling, and are not used in any physics solve. For CHT-only coupling, the mesh mirror only contains the boundaries to be coupled to MOOSE; otherwise, the mirror contains the entire CFD volume mesh. The mesh mirrors are built with either first- or second-order elements; the insets in Fig. 2 show the nodes created depending on the selected order.

The calculation workflow for each time step is as follows:

1. Read coupling data from the mesh mirror and interpolate into NekRS's internal arrays. For CHT coupling, a boundary heat flux q'' is applied to NekRS, while for volume coupling, a heat source q is applied to NekRS. In both cases, power is conserved through a normalization.

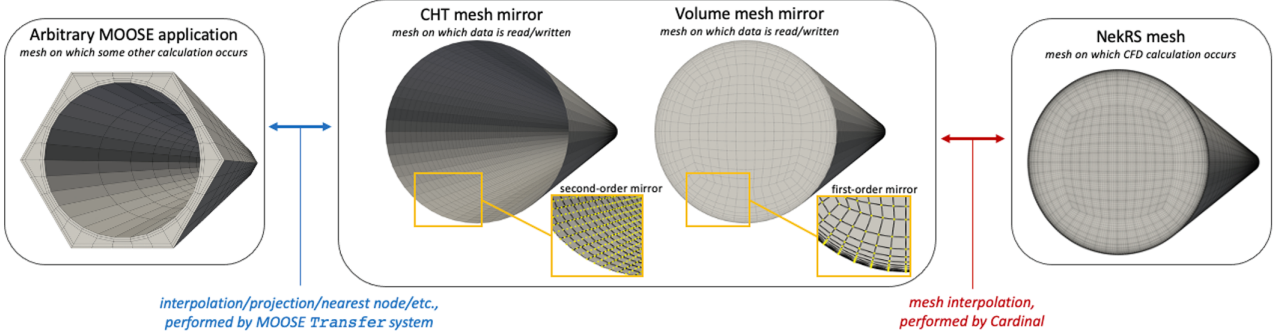


Fig. 2. Illustration of NekRS CFD mesh and the mesh mirrors used to facilitate data transfers.

2. Run NekRS for one time step.
3. Read coupling data from NekRS's internal arrays and interpolate onto the mesh mirror. For CHT coupling, a boundary temperature is written to the mirror, while for volume coupling, both temperature and density are written to the mirror.

The NekRS solution in element e , or f_e , is a linear combination of polynomials ϕ and coefficients c ,

$$f_e(x) = \sum_{i=0}^N c_i \phi_i(x), \quad (9)$$

where N is the polynomial order. In NekRS, the polynomials are Lagrange interpolants of GLL quadrature points, x_i for $0 \leq i \leq N$ such that $\phi_i(x_j) = \delta_{ij}$. To help explain the interpolation between NekRS's high-order solution and the lower-order mesh mirror, Fig. 3 shows a 1-D element with a third-order NekRS solution (the black curved line) based on four GLL points (blue dots). To interpolate this solution to a MOOSE element with arbitrary nodes p (red dots),

$$\begin{bmatrix} f(p_0) \\ f(p_1) \end{bmatrix} = \begin{bmatrix} \phi_0(p_0) & \phi_1(p_0) & \phi_2(p_0) & \phi_3(p_0) \\ \phi_0(p_1) & \phi_1(p_1) & \phi_2(p_1) & \phi_3(p_1) \end{bmatrix} \begin{bmatrix} c_0 \\ c_1 \\ c_2 \\ c_3 \end{bmatrix}. \quad (10)$$

This formulation is then extended to the problem-specific polynomial order.

After the solution is written to the mirror, the MOOSE Transfer system is used to transfer the fields to a coupled MOOSE application, where the NekRS solution may be used to apply BCs, set source terms, update material properties (such as cross sections), and so on. Note the very different discretizations on the pipe outer surface in Fig. 2 for the NekRS CFD mesh (right pane) and the

coupled MOOSE application's mesh (left pane). With many of MOOSE's transfer options, there are no requirements on node/element alignment between coupled models, which allows each code to use meshes most appropriate to its physics.

2.7. The OpenMC wrapping

Cardinal couples OpenMC to MOOSE through a volumetric kappa-fission tally (recoverable fission energy) and cross section feedback via temperatures and densities. Cardinal includes two options for tallying the fission power in OpenMC – 1) cell tallies or 2) libMesh unstructured mesh tallies. As for receiving physics feedback, because unstructured mesh tracking is currently under development, OpenMC's temperature and density feedback is applied to CSG cells.

The mesh mirror is created off-line using mesh generation software; in many cases, we simply use the coupled MOOSE application's mesh in order to avoid an extra mesh generation step, though this is not required. During initialization, Cardinal automatically loops over all the elements in the mesh mirror and maps by centroid to an OpenMC cell. Because the mesh mirror is only used for receiving data, no solve occurs on the mirror, so there are no requirements on node continuity across elements. Elements that don't map to an OpenMC cell simply do not participate in the coupling (and vice versa for the cells); this feature is used in the present work to exclude certain regions from multiphysics feedback, such as axial reflectors.

Fig. 4 shows an example of the OpenMC mesh mirror and the centroid-based spatial mapping used to couple OpenMC to a generic MOOSE application. The right-most pane shows an OpenMC CSG model, colored by cell ID. The left-most pane depicts the mesh for a generic coupled MOOSE application. The middle pane depicts the OpenMC mesh mirror; the colors represent the mapping of OpenMC cell IDs to the mesh mirror. The inset shows the actual boundary of an OpenMC cell as a white dashed line; the element centroids, shown as white dots, determine the cell-to-element mapping. There are no requirements on alignment of elements/cells or on preserving volumes – the OpenMC cells and mesh mirror elements do not need to be conformal.

Of course, any multiphysics simulation without *identical* meshes between code A and code B will suffer from a discretization error arising from solution interpolation between the codes. This applies equally to coupling Monte Carlo and heat transfer (the present application) as well as to coupling two mesh-based codes, such as neutron diffusion with heat conduction. The proper manner to address this discretization error is through a coupled physics mesh refinement study that ensures that all meshes, as well as the data communicated between applications, are sufficiently resolved. This work presents a coupled mesh refinement study in Section 5.4.

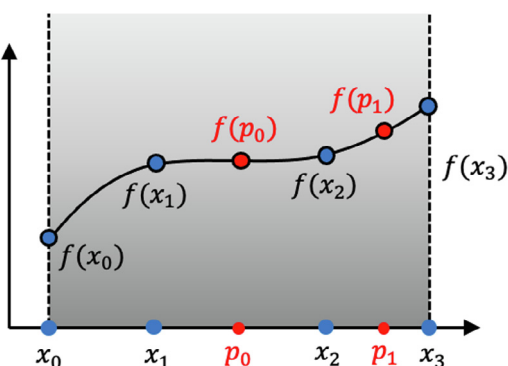


Fig. 3. Interpolation between a high-order NekRS solution (based on GLL quadrature points x) and generic points p .

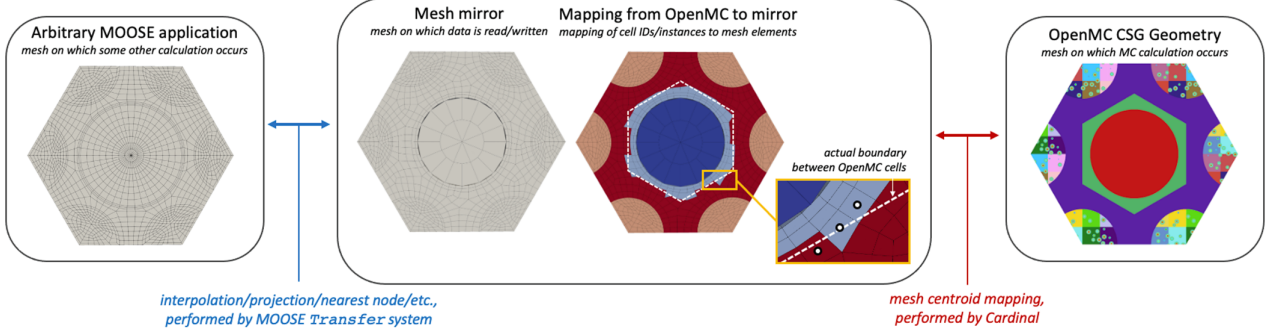


Fig. 4. Illustration of OpenMC particle transport geometry and the mapping of OpenMC cells to a user-supplied mesh (referred to as the “mesh mirror”).

Finally, for convenience, Cardinal automatically instantiates the tallies for all fissionable cells. The calculation workflow for each time step is as follows:

1. Read temperature and density from the mesh mirror; for each OpenMC cell, set its temperature and density to a volume average over that cell's corresponding elements.
2. Run a k -eigenvalue OpenMC calculation.
3. Read a kappa-fission tally from OpenMC's internal arrays and write onto the mirror using the cell-to-element mapping (for cell tallies) or element-to-element mapping (for unstructured mesh tallies). Power is conserved through a normalization.

After the solution is written to the mesh mirror, the MOOSE Transfer system is then used to transfer the fields to a coupled MOOSE application, where the OpenMC power distribution may be used to apply a volumetric heat source. Note that while the notion of “time steps” is used here, it should be understood that the OpenMC coupling in Cardinal is limited to pseudo-steady type calculations due to the use of a k -eigenvalue transport calculation. Instead of advancing in time, the notion of time stepping instead allows the frequency of the OpenMC solve to be customized and “sub-cycled” with respect to other coupled physics. Sub-cycling will be discussed in greater detail in Section 4.

Constant, Robbins-Monro, and Dufek-Gudowski (Dufek and Gudowski, 2006) relaxation schemes are available for the heat

source. In addition, Cardinal provides an interface to OpenMC's tally trigger system, which automatically terminates an OpenMC solve once reaching user-specified tolerances for standard deviation, variance, or relative error on k and the fission tallies (Shen et al., 2015). Cardinal also allows a sector-symmetric OpenMC model to map data symmetrically to a “full” domain to reduce cost; for example, an OpenMC model may consist of a 1/6th portion of a reactor core, but map tallies, temperatures, and densities to a full-domain mesh on which the T/H problem is solved.

3. The prototypic HTGR

This section describes the HTGR modeled in the present work. All geometric specifications, operating conditions, and material properties are loosely based on a collection of open source concepts, in particular a 2016 “point design” developed as part of a Department of Energy (DOE) initiative to explore high-temperature test reactors (Sterbentz et al., 2016). These design specifications are considered sufficiently representative of the HTGR class of reactors for the sake of demonstrating Cardinal's readiness for HTGR applications.

Two different geometries are modeled: a unit cell and a full core. Fig. 5 shows a top-down view of the full core, which is assembled by placing prismatic blocks in a hexagonal lattice. The design consists of 12 identical fuel assemblies, one central graphite reflector block, and an outer reflector of graphite blocks. The

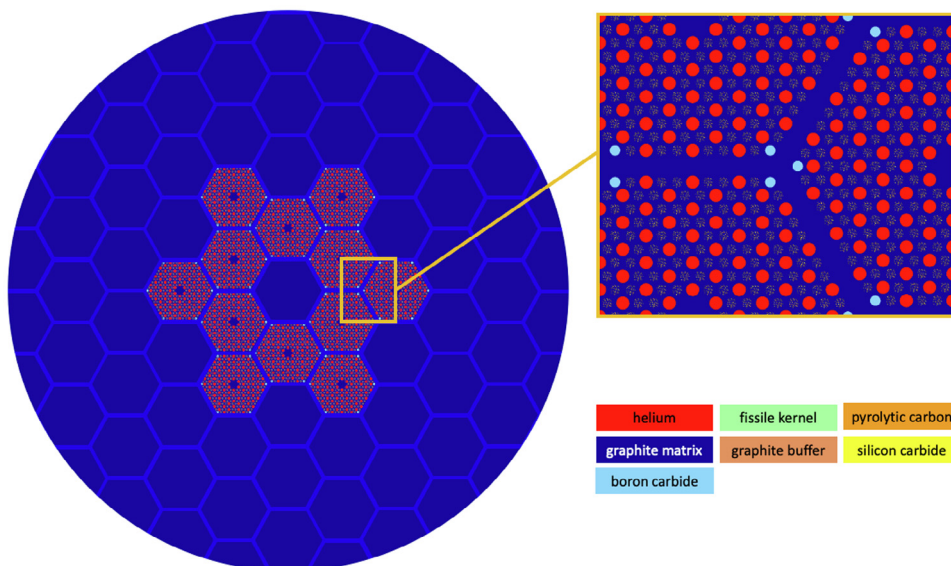


Fig. 5. Top-down view of the reactor. The edges of the hexagonal lattice are overlaid for visualization purposes.

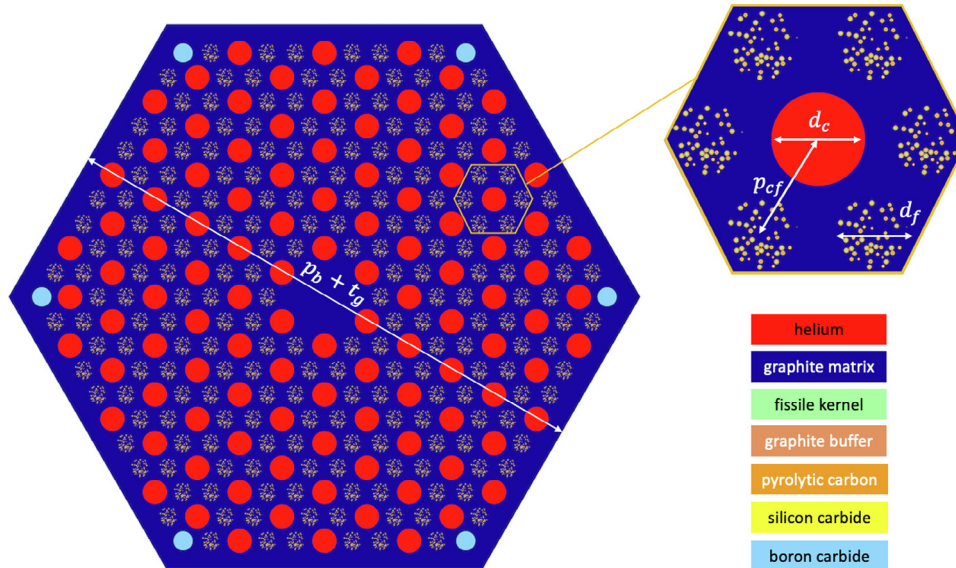


Fig. 6. Top-down view of a fuel assembly, colored by material.

hexagonal grid shown in Fig. 5 indicates the edges of the blocks. For simplicity, the reactor vessel is not considered; therefore, the model diameter is equal to the vessel inner diameter. On the top and bottom of the core are graphite reflectors; for simplicity, both are assumed to be of height L_r with a homogeneous mixture of 40% helium and 60% graphite. The only other major deviation taken from the 2016 point design is neglecting test-reactor-specific core structures such as irradiation access points and testing loops. By removing these structures, the fuel assemblies are also moved into a slightly different configuration to reduce leakage – the outer partial-ring of assemblies is shifted such that each assembly shares two faces with the inner ring of assemblies (as opposed to one shared face in the nominal design).

Fig. 6 shows a top-down view of a fuel assembly, which contains 108 helium coolant channels, 210 fuel compacts, and 6 burnable poison compacts. Each fuel compact consists of TRISO particles randomly dispersed in a graphite matrix with a packing fraction of 15%. A centrally-located partial-length fuel handling hole and four shallow dowel holes are neglected and replaced by graphite.

Modeling the in-core coolant bypass path through the mm-size gaps between assembly blocks is outside the present scope. Instead, the gaps are treated as solid graphite such that the effective assembly flat-to-flat distance is the assembly flat-to-flat distance p_b plus the assumed gap thickness t_g . The geometric parameters defining the core are summarized in Table 1.

The TRISO particles consist of a fissile kernel of uranium oxy-carbide with a $\frac{3}{2} : \frac{1}{2}$ ratio of carbon to oxygen (Fratoni, 2008). The kernel is successively enclosed in a carbon buffer, an inner Pyrolytic

Carbon (PyC) layer, a silicon carbide layer, and an outer PyC layer. The particle dimensions (Sterbentz et al., 2016) and material properties (Novak et al., 2021) are taken from the literature. The fuel is enriched to 15.5 w/o ^{235}U (Sterbentz et al., 2016), with a small poisoning of 0.2 w/o of ^{234}U assumed. The boron carbide poison compacts are defined with a 30 w/o ^{10}B enrichment in boron, with a total ^{10}B enrichment of 0.1 w/o (Sterbentz et al., 2016). All graphite materials are assumed to have the same composition as the matrix graphite.

Fig. 7 shows a top-down view of the unit cell geometry, a “coolant-centered” repeatable unit in an assembly. White dashed lines indicate the boundaries of the cylindrical fuel compacts. All geometric and material parameters are the same as for the full core case except that the height is taken as 1.6 m, or simply $100d_c$. The axial reflectors are also neglected. The operating conditions for the unit cell are obtained by normalizing the full core specifications by the total number of coolant channels, or 12 bundles \times 108 coolant channels per bundle, while also accounting for the reduced height.

Fission heat is removed by helium flowing downwards through the coolant channels. The power, inlet temperature, and other operating conditions for the full core and unit cell are summarized in Table 2.

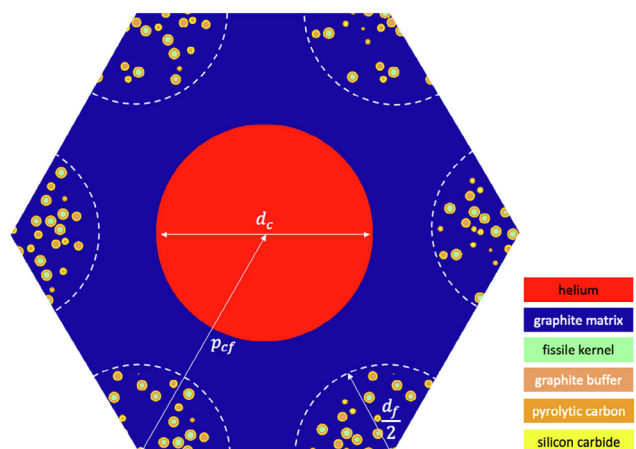


Fig. 7. Top-down view of the unit cell model.

Table 1

Geometric parameters defining the core and fuel assemblies (Sterbentz et al., 2016).

Parameter	Value
Coolant channel diameter, d_c	0.01588 m
Fuel and poison compact diameter, d_f	0.01270 m
Pitch between channel and compact, p_{cf}	0.01880 m
Bundle flat-to-flat distance, p_b	0.35996 m
Inter-assembly gap width, t_g	0.004 m
Active core height, L	6.343 m
Bottom reflector height, L_r	1.585 m
Top reflector height, L_t	1.585 m
Vessel inner diameter	3.3 m

Table 2

Operating conditions for the full core and unit cell models.

Parameter	Full Core Value	Unit Cell Value
Thermal power, q	200 MW	38.93 kW
Coolant inlet temperature, T_{inlet}	598 K	598 K
Coolant ΔT	325 K	82 K
Mass flowrate, \dot{m}	117.3 kg s ⁻¹	0.0905 kg s ⁻¹
Outlet pressure	7.1 MPa	7.1 MPa

4. Multiphysics coupling

OpenMC, BISON, NekRS, and THM are coupled via Picard iteration through MOOSE's MultiApp system, which places applications into a "tree," where each application may communicate with one application "above" it and N applications "below" it. All simulations in this work involve three codes – OpenMC, BISON, and NekRS/THM (depending on the thermal-fluid resolution). Fig. 8 shows the data transfers and MultiApp hierarchy used in the present simulation. Arrows indicate the communication between applications, while black numbered circles indicate the execution order in each iteration. Note that this work does consider multiphysics feedback from fluid density and temperature, even though these two effects are very small in HTGRs.

The two boxed insets indicate the different mesh representations used for NekRS (3-D) and THM (1-D). All fields are transferred using a nearest node transfer except for the wall heat flux sent to THM, which BISON instead averages in a number of axial layers for each channel. The average heat flux in layer i for coolant channel j is

$$q''_{ij} = \frac{\int_{z_{i-1}}^{z_i} q'' d\Gamma_j}{\int_{z_{i-1}}^{z_i} d\Gamma_j}, \quad (11)$$

where Γ_j is the boundary of the j -th channel wall. Robbins-Monro relaxation (Dufek and Gudowski, 2006) is applied to the heat source

in order to continually reduce the iteration-to-iteration relative change in the tallies as well as to improve stability. No relaxation is applied to the T/H fields.

Coupled convergence is assessed using MOOSE's automatic steady state detection features. Picard iterations continue until the relative L^2 norm of the auxiliary variable system is smaller than a user-specified tolerance. The auxiliary variable system in MOOSE is a single vector \vec{x} that contains the *entire* physics solution (solid temperature from BISON, fluid temperature and density from NekRS/THM, and fission distribution from OpenMC), with different applications updating portions of \vec{x} with each iteration. Conceptually, this can be represented as

$$\vec{x} = [\dot{q}_s \ T_s \ T_f \ \rho_f]^T, \quad (12)$$

where \dot{q}_s , T_s , T_f , and ρ_f themselves are vectors with lengths depending on the number of DOFs in each application. For a user tolerance of 10^{-3} , coupled convergence occurs when

$$\frac{\|\vec{x}^{(n)} - \vec{x}^{(n-1)}\|_2}{\|\vec{x}^{(n-1)}\|_2} \leq 10^{-3}. \quad (13)$$

Picard iterations are achieved "in time." In other words, the overall Cardinal simulation has a notion of "time" and a time step index, but only NekRS is actually solved with non-zero time derivatives. The notion of time-stepping is then used to customize how frequently (i.e., in units of time steps) data is exchanged among applications. Each application uses a unique time step size, which improves stability and reduces the number of high-cost solves and data transfers. To help explain the strategy in Cardinal, represent the time step sizes in NekRS, BISON, and OpenMC as Δt_{nek} , $\Delta t_{\text{bison}} = M\Delta t_{\text{nek}}$, and $\Delta t_{\text{openmc}} = NM\Delta t_{\text{nek}}$, respectively. Selecting $N \neq 1$ and/or $M \neq 1$ is referred to as "sub-cycling." In other words, NekRS runs M times for each BISON solve, while BISON runs N times for each OpenMC solve, effectively reducing the total number of BISON solves by a factor of M and the total number of

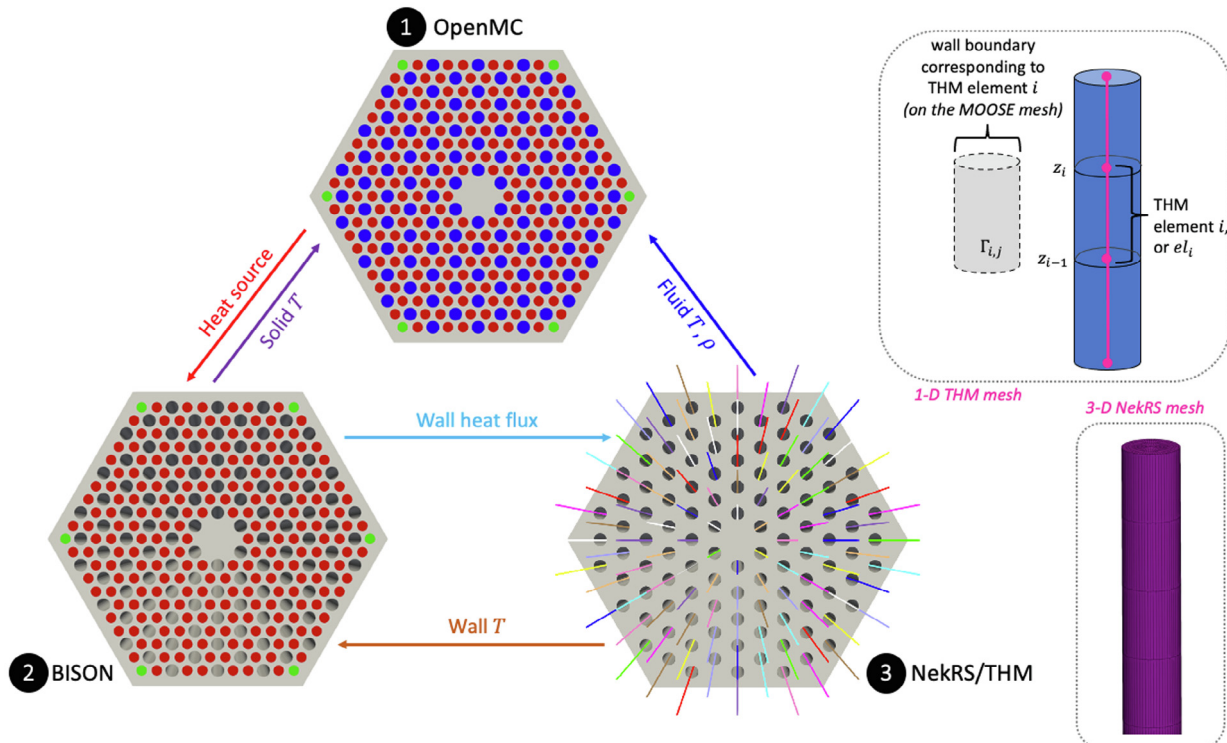


Fig. 8. Data transfers used for coupling NekRS/THM, BISON, and OpenMC for a fuel assembly. The meshes used by NekRS and THM are shown in magenta in the two insets. Black numbered circles indicate the execution order in each iteration.

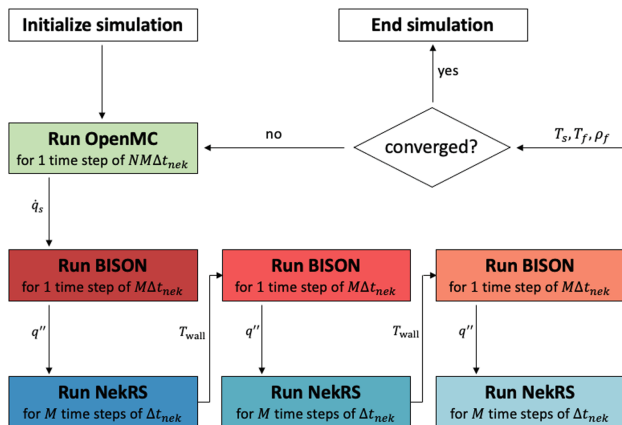


Fig. 9. Coupling procedure with subcycling for a calculation with OpenMC, BISON, and NekRS for $N = 3$.

OpenMC solves by a factor of NM compared to the naive approach to exchange data based on the smallest time step across the coupled codes. Each Picard iteration consists of:

1. Run an OpenMC k -eigenvalue calculation. Transfer \dot{q}_s to BISON.
2. Repeat N times:
 - (a) Run a steady-state BISON calculation. Transfer q'' to NekRS.
 - (b) Run a transient NekRS calculation for M time steps. Transfer T_{wall} to BISON.
3. Transfer T_s , T_f , and ρ_f to OpenMC.

A similar strategy is also used in the THM-based coupling. Fig. 9 shows the procedure for an example selection of $N = 3$, meaning that the BISON-NekRS sub-solve occurs three times for every OpenMC solve.

In the present work, $M = 50$ and $N = 100$ are selected based on preliminary scoping studies; a rigorous search for the optimal choices of N and M is deferred to future work.

5. Unit cell simulations

This section presents coupled physics simulations of the HTGR unit cell. Various combinations of codes are used to highlight Cardinal's plug-and-play infrastructure and assess the needed thermal-fluid resolution for the later full-core simulations. First, Section 5.1 describes the single-physics models developed for OpenMC, NekRS, THM, and BISON. Then, Section 5.2 presents CHT coupling of NekRS/THM and BISON, where the high-resolution NekRS simulations are used to generate a corrected Nusselt number model for THM.

Next, Section 5.3 presents coupled physics predictions of NekRS-BISON-OpenMC and THM-BISON-OpenMC. Finally, Section 5.4 discusses the mesh refinement studies used to ensure appropriate convergence of the meshes, cells, and tallies for the simulations in Sections 5.2 and 5.3. While mesh convergence studies are usually presented upfront, in this case there are interesting observations regarding the OpenMC model refinement that are best discussed after already understanding the coupled physics predictions.

5.1. Single-physics models

5.1.1. OpenMC model

The OpenMC model is shown in Fig. 10. Periodic BCs are applied to the six lateral faces, with vacuum BCs on the top and bottom faces. The number of particles per batch is fixed at 200000 and the Shannon entropy is used to select the number of inactive batches (Brown, 2006). OpenMC's tally trigger system is then used to terminate each Picard iteration once the maximum relative uncertainty (based on $1-\sigma$ standard deviations) in the fission distribution is less than 1%.

To accelerate the particle tracking, a Cartesian lattice is superimposed in the TRISO regions. Note the difference between this Cartesian lattice (visible in the leftmost image in Fig. 10) and the cell tally discretization (visible in the rightmost image in Fig. 10). The Cartesian lattice has no effect on the physics model, and is only added to improve performance by limiting the number of cells to search for each particle lookup.

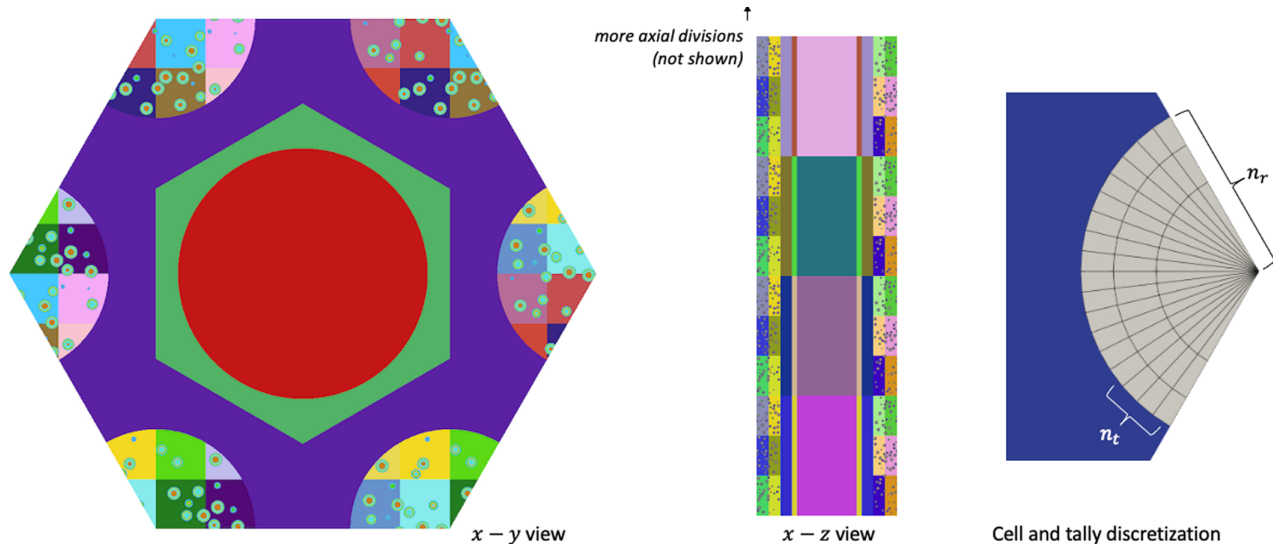


Fig. 10. OpenMC unit cell model on an $x-y$ plane (left) and an $x-z$ plane (middle), colored by cell ID. The cell and tally discretization is shown on the right, but is not visible in the $x-y$ and $x-z$ views.

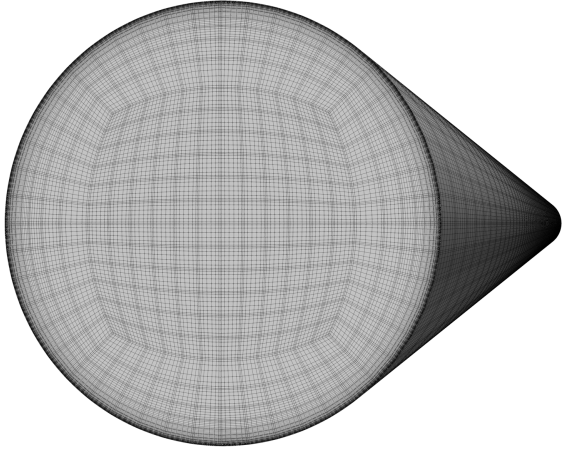


Fig. 11. Top-down view of the NekRS mesh; lines are shown connecting the GLL quadrature points.

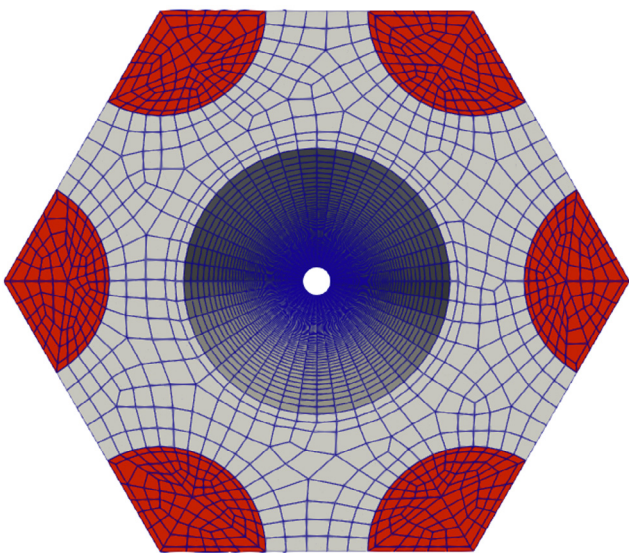


Fig. 12. Top-down view of the BISON mesh.

In the axial direction, the geometry is divided into n_l layers of equal height. In the radial and azimuthal directions, the fuel compacts are further subdivided into n_r radial cells and n_t azimuthal cells of equal volume. A converged OpenMC simulation in this case is obtained with $n_r = 4$, $n_t = 1$, and $n_l = 50$. For simplicity, the tally discretization is set to the same discretization as the cells. Examples of Cardinal applications using mesh tallies are available elsewhere (Novak et al., 2022; Merzari et al., 2021).

Due to the symmetry and the large numbers of tallies used to obtain reference solutions in the mesh convergence studies in Section 5.4, the unit cell is constructed as a 1/6th symmetric version of Fig. 10. Cardinal's utilities are then used to apply symmetric mappings to a full-domain coupled MOOSE mesh. Therefore, each OpenMC model contains a total of $n_r n_t n_l = 200$ tallies and receives $n_r n_t n_l + 3n_l = 350$ unique cell temperatures and $n_l = 50$ unique fluid densities from BISON and NekRS/THM.

Cardinal provides high flexibility for the geometric “level” on which temperatures and densities are coupled to OpenMC. If the coupled MOOSE application resolves TRISO particles, very fine temperature coupling can be applied by mapping to the individual OpenMC cells defining the TRISOs. Because the present application homogenizes the TRISO particles in the heat conduction model, Cardinal instead applies temperature feedback at a “higher” level in the geometry, such that all cells contained within each higher-level cell are set to the same temperature. In other words, if a TRISO particle happens to straddle one of the cell divisions shown in Fig. 10, those TRISO cells are geometrically split along the boundary such that the portion of the TRISO particle in cell A is set to T_A and the portion of the TRISO particle in cell B is set to T_B .

5.1.2. NekRS model

The NekRS model is shown in Fig. 11. The NekRS model development is separated into two distinct phases. First, a periodic pipe with a height equal to 1/10 of the nominal unit cell height is used to solve the isothermal $k\text{-}\tau$ RANS model. In the second phase, this periodic flow solution is extrapolated to the full domain height and “frozen” such that only the transport of temperature (given μ_T and \vec{V} from the periodic solution) is solved. For the full-height case, the inlet is uniform temperature and the outlet is uniform pressure; walls are no-slip with heat flux provided by BISON. This phased approach results in a cost savings of about 100× (10× due to the shortened-height, and another 10× due to the order of magnitude cheaper passive scalar solver compared to the pressure–velocity solver).

5.1.3. THM model

The THM model is a 1-D pipe with a constant inlet mass flow-rate and temperature and constant outlet pressure. Because the cost of the THM solve is very small compared to the other tools, the mesh is selected to simply have an equal number of axial elements as the BISON mesh. Each THM element receives a wall heat flux from BISON.

5.1.4. BISON model

A top-down view of the BISON mesh is shown in Fig. 12. All boundaries are insulated except the coolant channel surface, where a Dirichlet wall temperature BC given by NekRS/THM is imposed. The TRISO particles are homogenized into the compacts.

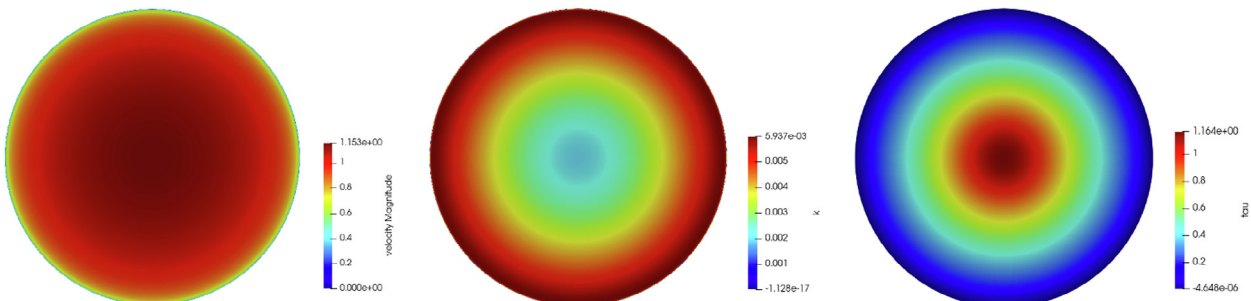


Fig. 13. NekRS predictions of velocity magnitude (left), k (middle), and τ (right), all in non-dimensional units, on an x - y plane.

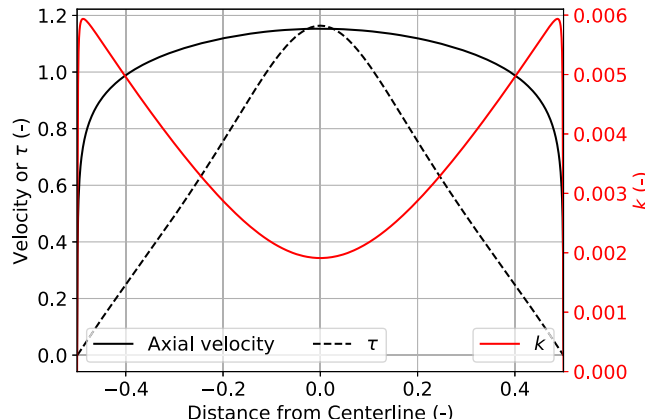


Fig. 14. NekRS predictions of the axial velocity, k , and τ , all in nondimensional units, on a line through the center of the pipe.

5.2. Conjugate heat transfer

This section presents CHT coupling of NekRS–BISON and THM–BISON for the unit cell. The first objective is to generate a corrected Nusselt number model for THM using NekRS. The second objective is to then gradually increase physics complexity before incorporating Monte Carlo feedback in Section 5.3. In this section, the power distribution is set as a radially-uniform, sinusoidal function of height.

Fig. 13 shows the velocity magnitude, k , and τ predicted by NekRS. Because the flow solution is obtained from a periodic model, these solutions represent fully-developed flow, and are constant along the main flow direction. Fig. 14 shows the same fields on a line spanning the channel cross-section. All quantities display the expected physical behavior: the peak axial velocity is about 1.15 times the uniform inlet velocity, k reaches a peak very close to the wall and decreases towards the centerline, and τ peaks at the centerline.

Fig. 15 shows the solid temperature predicted by NekRS–BISON, THM–BISON, and the difference (NekRS minus THM). Temperatures are highest in the six compact regions, slightly downstream from the core midplane due to the combined effects of convective heat transfer and the imposed power distribution. The solid temperature distributions agree very well with each other – the max-

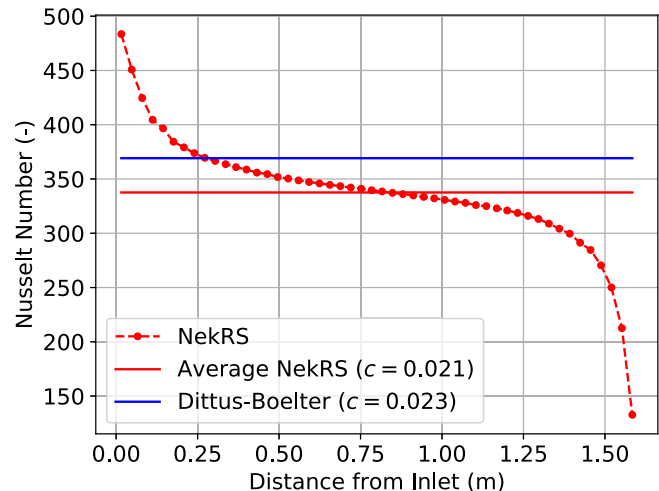


Fig. 16. Nusselt number as a function of distance from the inlet for NekRS.

imum solid temperature difference is 17.2 K, which can be attributed to at least two sources:

- THM averages q'' along the channel perimeter, so THM is incapable of representing the azimuthal variation in wall heat flux.
- NekRS resolves thermal and momentum boundary layers, whereas THM uses the Dittus-Boelter and Churchill correlations, respectively. Assuming no other competing effects, a 17.2 K difference is equivalent to about a 10% difference in convective heat transfer coefficient. Errors as high as 25% may be observed when using a simple model such as the Dittus-Boelter correlation (Incropera and Dewitt, 2011), and a 10% difference is well within the realm of the data scatter used to originally fit the Dittus-Boelter model (Winterton, 1998).

A common multiscale use case of NekRS is the generation of closures for lower-order tools. Here, NekRS is used to correct the THM closures to better reflect the conditions of interest. Due to limited scope, a correction is only computed at the Reynolds and Prandtl numbers characterizing the unit cell ($Re = 223214$ and $Pr = 0.655$). That is, a new coefficient c is computed for a correlation with the same functional dependence as the Dittus-Boelter correlation,

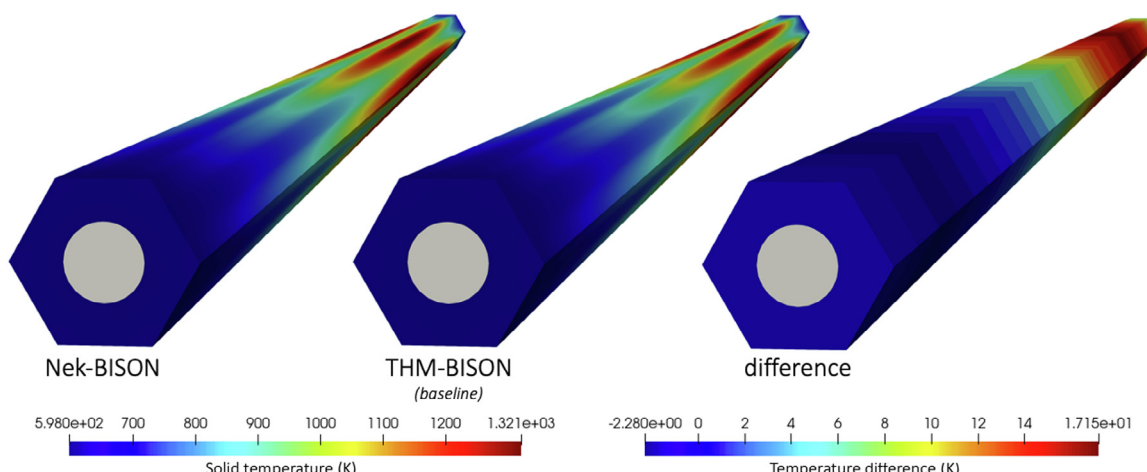


Fig. 15. Solid temperature predicted for CHT coupling of NekRS–BISON, THM–BISON, and the difference (NekRS minus THM). Difference is shown with a constant monomial basis to improve clarity.

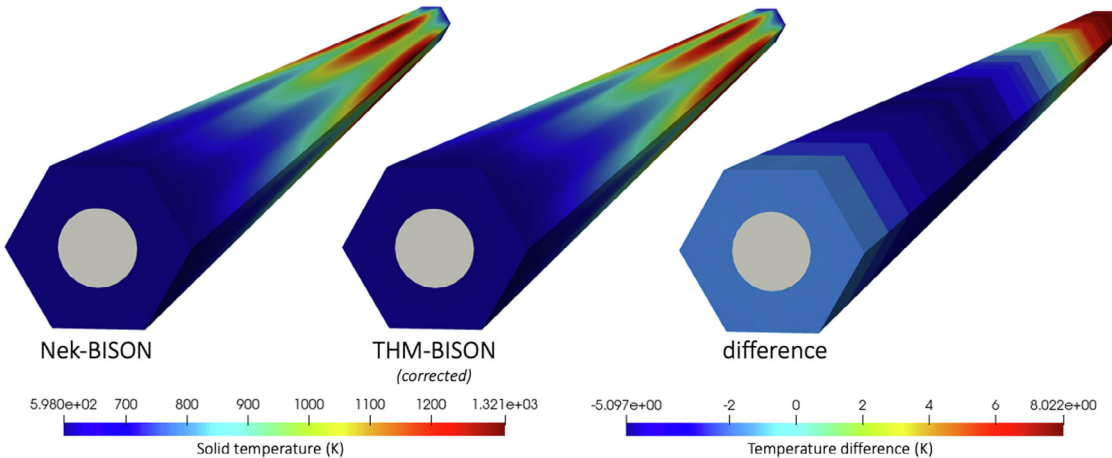


Fig. 17. Solid temperature predicted for CHT case for NekRS–BISON, corrected THM–BISON, and the difference between the two (NekRS minus corrected THM).

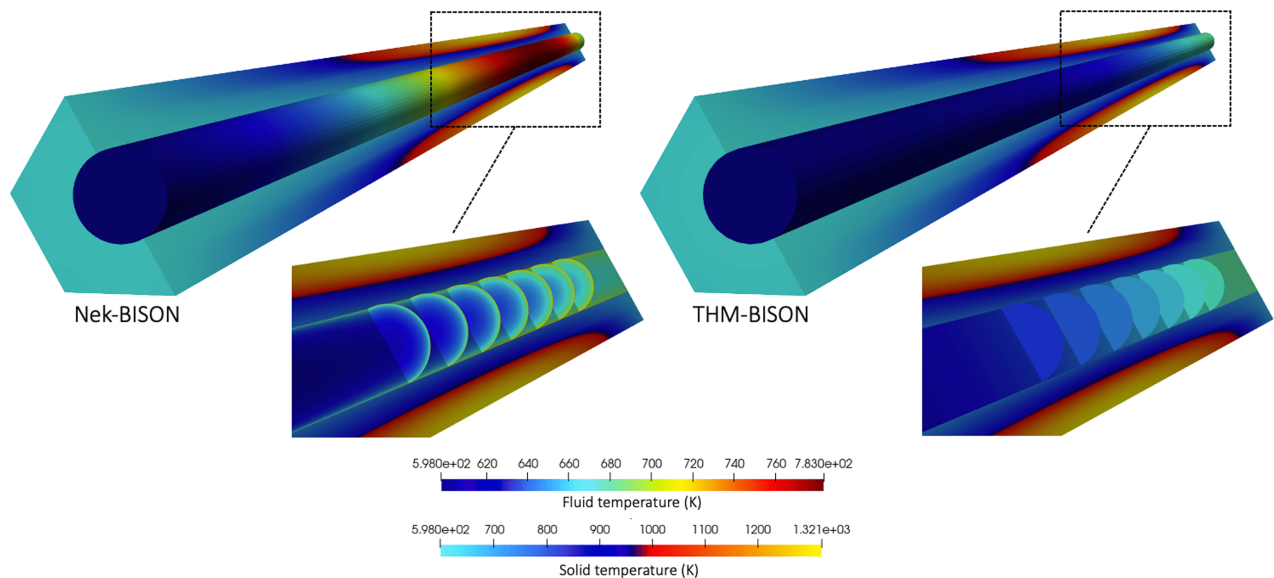


Fig. 18. Fluid temperature predicted for CHT coupling of NekRS–BISON and THM–BISON.

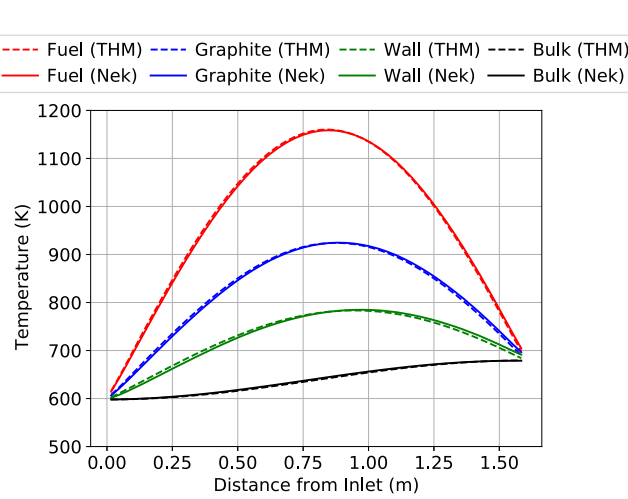


Fig. 19. Radially-averaged temperatures for the NekRS–BISON and THM–BISON CHT simulations.

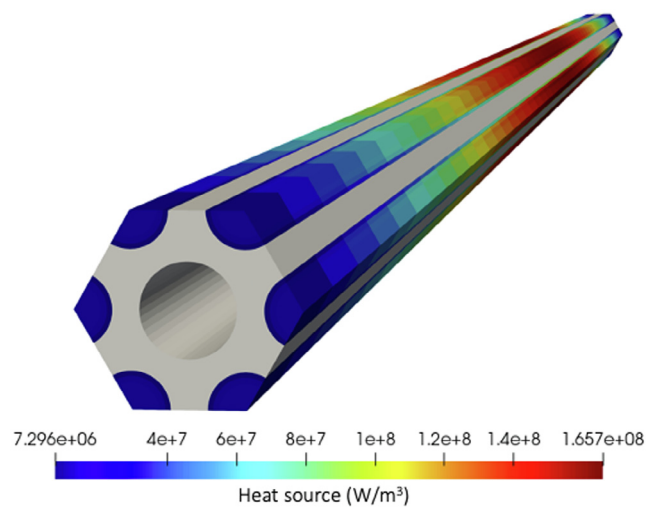


Fig. 20. Heat source predicted by OpenMC for the NekRS–BISON–OpenMC simulation.

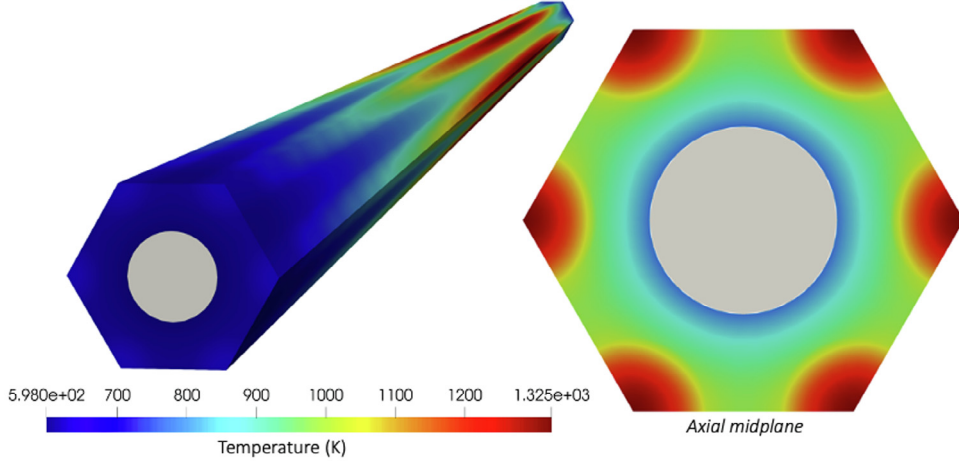


Fig. 21. Solid temperature predicted by BISON for the NekRS–BISON–OpenMC simulation.

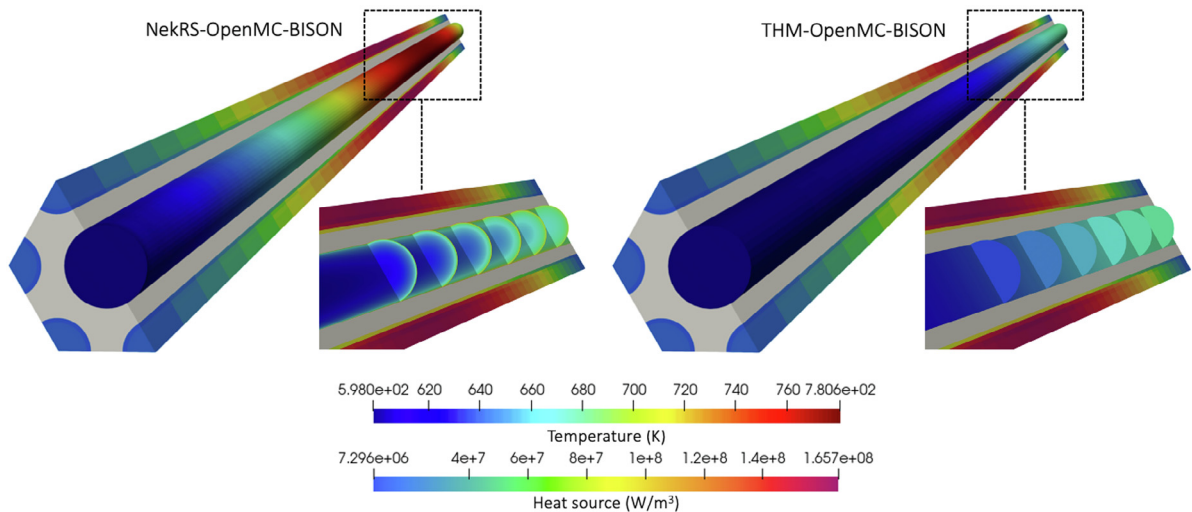


Fig. 22. Fluid temperature predicted by NekRS and THM for the coupled simulation. For each case, the OpenMC power distribution is shown on a separate color scale.

$$Nu = cRe^{0.8}Pr^{0.4}. \quad (14)$$

The heat transfer coefficient is computed in a series of layers along the flow direction as

$$q''_i = h_i(T_{\text{wall},i} - T_{\text{bulk},i}), \quad (15)$$

where an i subscript denotes a quantity pertaining to layer i , q'' is the average wall heat flux, h is the heat transfer coefficient, T_{wall} is the average wall temperature, and T_{bulk} is the volume-averaged temperature. Cardinal contains a mature postprocessing system to directly extract the quantities in Eq. (15) from a NekRS solution.

Fig. 16 shows the Nusselt number computed by NekRS. The average NekRS Nusselt number is 8.5% smaller than the Dittus–Boelter correlation, which agrees well with the previous qualitative assessment. Based on Fig. 16, the THM input file is modified to use $c = 0.021$ for the Dittus–Boelter correlation, and the THM–BISON simulations are repeated.

Fig. 17 compares the solid temperature predicted by NekRS–BISON and the corrected THM–BISON simulation; the maximum solid temperature difference decreases to 8.0 K. The average magnitude of the temperature difference is only 4.7 K, which is a very successful outcome considering that the NekRS mesh has roughly 1 million times as many DOFs as the THM mesh. NekRS's capability for resolving the azimuthal variation in channel heat flux is incon-

— Fuel T (THM)	— Wall T (THM)	— Power (THM)
— Fuel T (Nek)	— Wall T (Nek)	— Power (Nek)
— Graphite T (THM)	— Bulk T (THM)	
— Graphite T (Nek)	— Bulk T (Nek)	

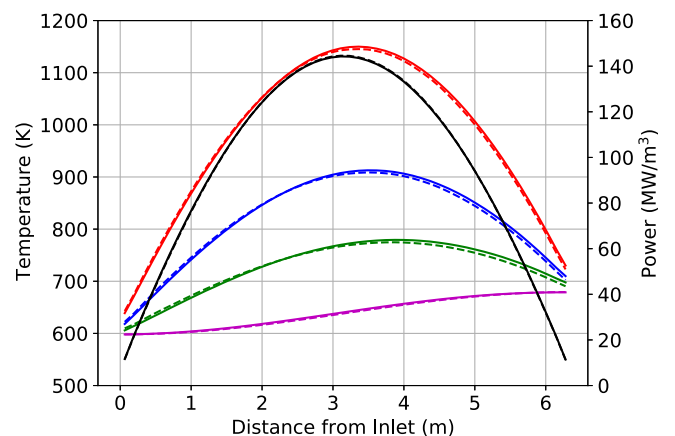


Fig. 23. Radially-averaged temperatures and power for the NekRS–BISON–OpenMC and THM–BISON–OpenMC simulations.

sequential for this unit cell application. All subsequent THM simulations in this work use the corrected Dittus–Boelter model.

Fig. 18 shows the fluid temperature predicted by NekRS–BISON and THM–BISON. Also shown for context is the solid temperature in a slice through the domain, on a different color scale. The NekRS simulation resolves the thermal boundary layer, whereas the THM model uses the Dittus–Boelter correlation to represent the temperature difference between the wall and the bulk. Therefore, the THM fluid temperature shown in **Fig. 18** is the area-averaged fluid temperature. The wall temperature predicted by NekRS follows a similar distribution as the heat flux, peaking slightly downstream of the midplane due to the combined effects of convective heat transfer and the imposed power distribution.

Finally, **Fig. 19** compares various radially-averaged temperatures along the flow direction. As already discussed, the solid temperatures match very well between NekRS–BISON and THM–BISON and also match the expected behavior for a sinusoidal power distribution. Given the insignificant differences between NekRS or THM based T/H feedback, the inclusion of neutron transport physics in the next section is again expected to yield very small differences.

5.3. Multiphysics coupling

In this section, multiphysics coupling of NekRS/THM, BISON, and OpenMC is performed for the unit cell. In the previous section, when an identical heat source distribution was imposed for CHT simulations, there was on average only a 4.7 K difference in solid temperature and a 1.3 K difference in area-averaged fluid temperature between simulations conducted with NekRS or THM. The average difference in fluid density was also very small, at only 0.02 kg m^{-3} . These differences are too small to result in any significant differences once incorporating OpenMC feedback, aside from the inherent statistical uncertainty in the OpenMC solution and NekRS's 3-D representation of the fluid domain. This expectation was indeed observed here; therefore, for brevity, most simulation results presented in this section only depict the NekRS–BISON–OpenMC predictions.

Convergence was obtained in four Picard iterations; no instabilities were observed among the physics. **Fig. 20** shows the fission power predicted by OpenMC. Due to the relatively low fluid temperature rise of 82 K, the power distribution is nearly symmetric about the axial mid-plane. There is a thin low-power region near the edge of the compact that arises from the TRISO sphere distribution, which will be discussed in greater detail in Section 5.4. The maximum percent difference in power between the NekRS and THM cases is only 1.3%, which is of similar magnitude as the imposed maximum relative tally uncertainty of 1%.

Fig. 21 shows the solid temperature predicted by BISON. The solid temperature peaks slightly downstream of the maximum power due to the combined effects of the power distribution and convective heat transfer at the wall. The cell-wise fission power from OpenMC introduces some piecewise nature to the solid temperature, though axial diffusion does smooth the effect. The maximum solid temperature difference between the NekRS and THM cases is 5.4 K.

Fig. 22 shows the fluid temperature predicted by NekRS and THM, with the OpenMC power distribution shown on a separate color scale. NekRS resolves the thermal boundary layer, whereas the THM model uses the Dittus–Boelter correlation to represent the temperature drop from the heated wall to the bulk. Therefore, the THM fluid temperature shown in **Fig. 22** represents the area-averaged fluid temperature. The wall temperature predicted by NekRS follows a similar distribution as the heat flux, with a profile that peaks slightly downstream of the maximum power due to the

combined effects of convective heat transfer and the fission power distribution.

Fig. 23 compares the radially-averaged temperatures along the flow direction between the NekRS–BISON–OpenMC and THM–BISON–OpenMC cases. Note the use of separate axes for temperatures (left) and power (right). The solid and fluid temperatures match very well between the two thermal-fluid feedback options.

Altogether, an excellent agreement was obtained between the NekRS–BISON–OpenMC and THM–BISON–OpenMC coupled physics simulations, even though the NekRS model used about 1.35×10^8 DOFs for temperature but the THM model only used 1.5×10^2 DOFs for temperature. With a calibrated Nusselt number model, the maximum solid temperature difference is only 5.4 K. Given the limitations of this model neglecting interassembly flow, resolution of the momentum and energy boundary layers with a 3-D RANS model is not required to capture the coupled neutronics-T/H physics in an infinite lattice of the present HTGR's unit cells. Therefore, all full-core simulations in Section 6 will use THM.

5.4. Mesh refinement study

This section describes the refinement studies pursued to determine suitable 1) OpenMC cell and tally discretization, 2) NekRS polynomial order, and 3) BISON mesh refinement used in the unit cell simulations. For brevity, most discussion will emphasize the methods and criteria for evaluating convergence rather than presenting convergence plots directly. For OpenMC, several interesting observations related to TRISO fuels motivate more in-depth discussions.

5.4.1. NekRS refinement

Because the NekRS mesh is much finer than the other physics tools, the NekRS mesh refinement study is conducted independently of a coupled simulation. Mesh convergence was assessed by running the RANS case for $N = 3, 5, 7$, and 13 with near-wall refinement to ensure that $y^+ < 1$. Mesh-independence of the pressure, velocity, k , and τ was obtained for $N = 7$. The converged mesh contains 2.62×10^5 elements, or about 1.34×10^8 GLL points.

5.4.2. OpenMC refinement

While the NekRS refinement was conducted in a single-physics sense, all OpenMC model refinement studies are conducted with a coupled THM–BISON–OpenMC model in order to resolve the multiphysics effects on mesh convergence. For brevity, the OpenMC discretization is presented as $n_{r/t/l}$; for example, $n_{8/4/100}$ represents a model with $n_r = 8$ radial cells, $n_t = 4$ azimuthal cells, and

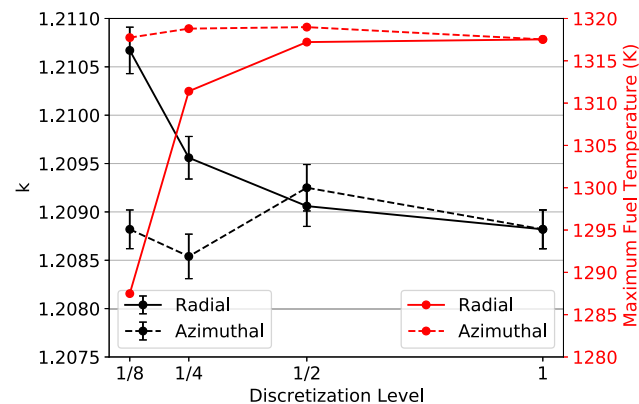


Fig. 24. k and the maximum fuel temperature as a function of OpenMC model refinement.

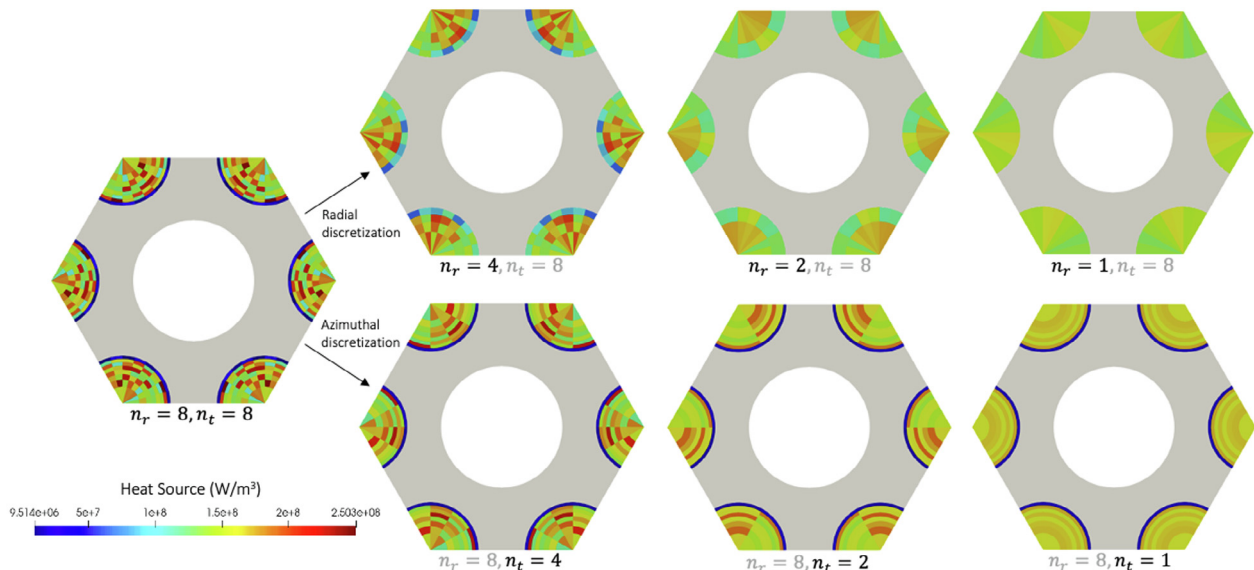


Fig. 25. OpenMC fission distribution on the axial midplane as a function of radial (top row) and azimuthal (bottom row) refinement of the OpenMC model.

$n_l = 100$ axial cells. Convergence is explored by individually varying n_r , n_t , and n_l and comparing to a reference solution obtained for $n_{8/8/100}$.

Convergence is defined as the point when 1) k is within 3σ of the reference and 2) the maximum fuel temperature is within 10 K of the reference. The criteria for T/H convergence should technically account for the propagation of the Monte Carlo uncertainty to the T/H solve (Ferraro et al., 2019), but our previous studies suggest that 10 K is much greater than the propagated uncertainty and simplifies the work. Other criteria including graphite and fluid temperatures were also considered but ultimately did not vary significantly with discretization.

First, the cross-plane discretization of the OpenMC model is explored by individually varying n_r and n_t for a fixed $n_l = 100$. Fig. 24 shows k and the maximum fuel temperature as a function of refinement. On the x axis, unity represents the finest discretization level, while fractions represent coarser models. For example, with the azimuthal refinement curves, unity indicates $n_{8/8/100}$ (the finest azimuthal refinement) and 1/8 represents $n_{8/1/100}$ (the coarsest azimuthal refinement, which has 8× less azimuthal elements than the reference). In other words, models become more finely discretized when moving from left to right on the x axis. The convergence criteria do not vary significantly with azimuthal refinement, and the model is sufficiently converged with just a single azimuthal region. Conversely, as the radial mesh is refined, k decreases and the maximum fuel temperature increases; four radial regions are sufficient to reach convergence.

To understand these trends, Fig. 25 shows the OpenMC fission distribution on the midplane as a function of radial (top row) and azimuthal (bottom row) refinement. Because the TRISO particles do not intersect the compact surface, there is a zero power region of thickness $(d_p - d_k)/2$ at the compact boundary, where d_p is the particle diameter and d_k is the kernel diameter. In LWRs, the “rim effect” results in the highest powers directly at the fuel surface (Suikkanen et al., 2020), whereas in TRISO fuels the peak power is offset slightly into the volume. As the radial refinement increases, the zero-power periphery region is better resolved. This redistribution in power results in higher peak fuel temperatures because the thermal resistance between the fuel and the coolant increases with radial refinement. In systems with negative temperature coefficients, the

inward shift of the power distribution increases peak temperatures, reducing k .

With a cell-based tally, the random TRISO packing contributes to the observed bin-to-bin differences in power. For small tally bins, it becomes possible for zero or very few TRISO particles to fall within a particular bin, causing high bin-to-bin variations in power. For instance, Fig. 26 shows the $n_{8/8/100}$ heat distribution from Fig. 25 overlaid with the actual TRISO particle locations in each bin. The diameter of the circles is equal to the kernel diameter, indicating the heat-generating regions. The bins with more TRISOs particles correspond to the higher powers. Additional simulations with very high numbers of particles further confirm that the bin-to-bin variations indeed result from the random TRISO distribution and, to a lesser extent, spatial self-shielding.

Next, the axial discretization of the OpenMC model is explored by individually varying n_l for fixed $n_r = 8$ and $n_t = 8$. Axial convergence is assessed once the relative L^2 norm of the radially-averaged fuel temperature is less than 0.5%. The relative L^2 norm between 50 and 100 layers is 0.09%, such that convergence is obtained with $n_l = 50$.

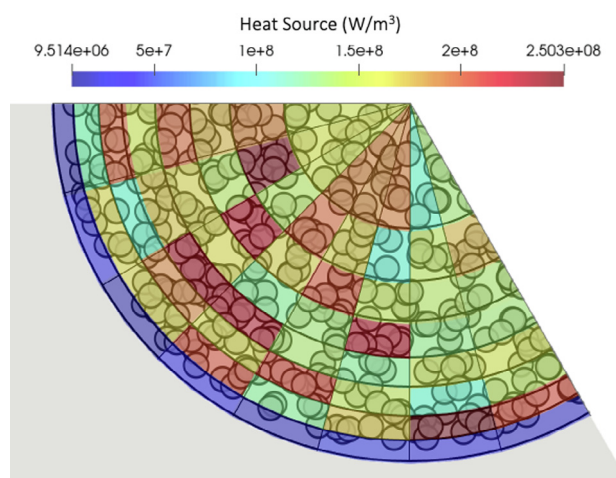


Fig. 26. TRISO particles superimposed on the fission distribution in one layer of the OpenMC model.

5.4.3. BISON refinement

Similar to the OpenMC case, the BISON mesh refinement study is conducted with a coupled THM–BISON–OpenMC model in order to resolve the multi-physics effects on mesh convergence. Convergence between successively refined BISON meshes is assessed once the relative L^2 norm of the radially-averaged fuel and block temperatures is less than 0.5%. Between the mesh in Fig. 12 and a uniformly-refined version of the same mesh, the relative L^2 norms

of the fuel and block temperatures are 0.29% and 0.23%, respectively. As both of these quantities meet the defined convergence criteria, the coarser mesh shown in Fig. 12 was used.

6. Full core simulations

This section presents coupled physics simulations of a full-core prismatic HTGR using OpenMC, THM, and BISON. THM is selected

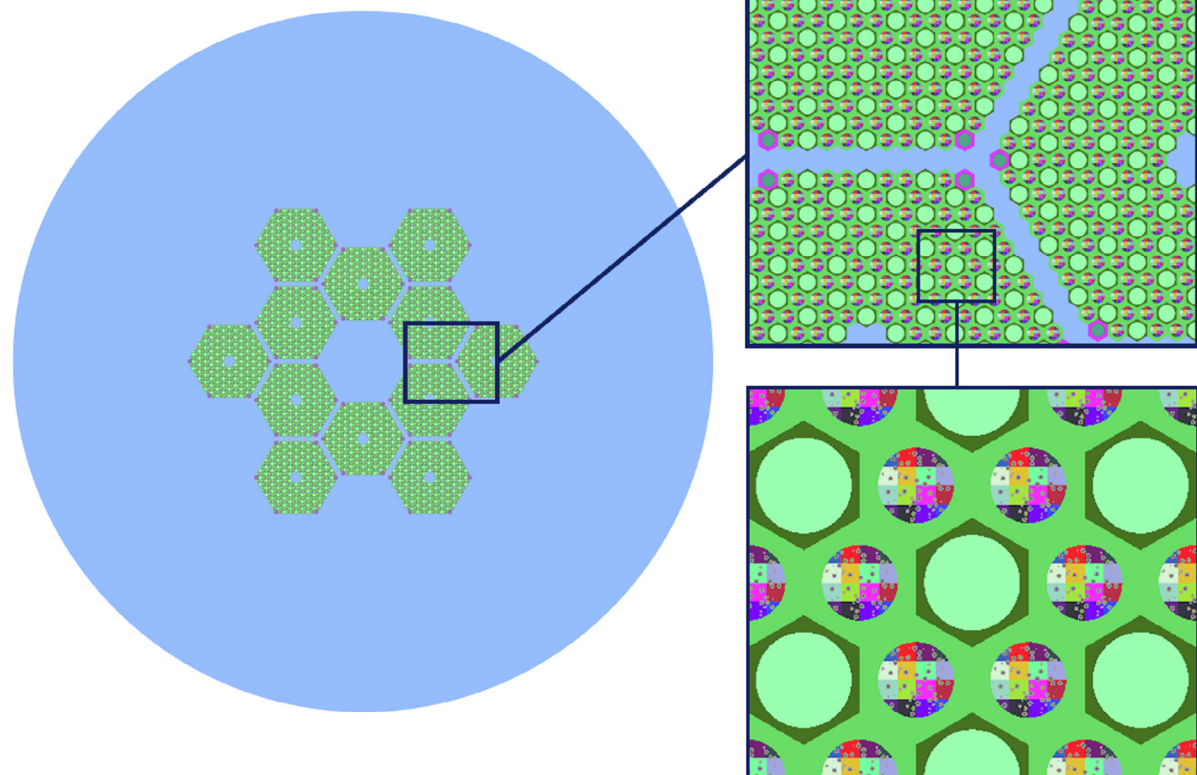


Fig. 27. OpenMC model on the $x - y$ plane, colored by cell ID. The cell and tally discretization in the compacts is not shown.

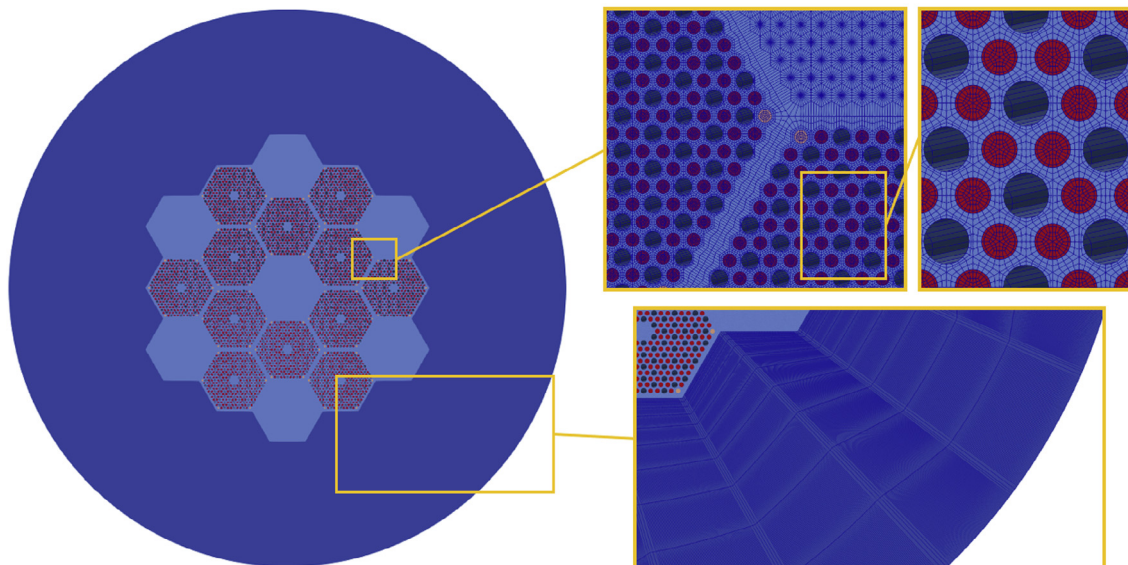


Fig. 28. Top-down view of the BISON mesh.

as the thermal-fluid modeling tool based on the unit cell simulations in Section 5, which demonstrated that THM's 1-D flow models are excellent approximations to the flow channels in the HTGR of interest, with only very small differences from 3-D wall-resolved RANS models.

First, Section 6.1 describes the “single-physics” models developed for OpenMC, THM, and BISON. Identical mesh convergence studies as described in Section 5.4 for the unit cell are applied to the full core model but for brevity are not discussed. Then, Section 6.2 presents multiphysics coupling of THM, OpenMC, and BISON for the full core geometry.

6.1. Single physics models

6.1.1. OpenMC model

The OpenMC CSG model is shown in Fig. 27. Vacuum BCs are applied to all outer boundaries. The number of particles per batch is fixed at 200000 and the Shannon entropy is used to select the number of inactive batches. OpenMC's tally trigger system is again used to terminate each OpenMC solve once reaching less than 1% maximum relative uncertainty in the fission distribution.

The geometry is divided into $n_l = 50$ layers of equal height. The main impact of radial discretization is resolution of the low-power “rim” in the TRISO compacts; as was seen in Section 5, the power displayed fairly small ring-to-ring variations for rings in the compact interior. Therefore, the OpenMC model is here divided into $n_r = 2$, with the outer ring having 1/3 the volume of the inner ring. Even though greater azimuthal variation in power occurs for the full core geometry due to asymmetric poisoning and moderation, the cell and tally refinement study suggests converged results even with a single azimuthal zone, or $n_t = 1$.

Due to the core symmetry, the OpenMC model is again constructed as a 1/6th-symmetric version of Fig. 27, with Cardinal's

mapping utilities used to apply symmetric mappings of the heat source, temperatures, and densities to a full coupled MOOSE mesh. Therefore, the OpenMC model consists of 42000 tallies.

6.1.2. THM model

The THM model consists of 210×12 separate coolant channels with the same BCs as the unit cell case in Section 5.1.3. Because the cost of the THM solve is very small compared to the other tools, the mesh of each channel is simply selected to have an equal number of axial elements as the BISON mesh.

6.1.3. BISON model

A top-down view of the BISON mesh is shown in Fig. 28. This mesh is constructed using the MOOSE reactor module, which contains utilities for meshing common reactor core geometries, such as quadrilateral and hexagonal lattices of pins, ducts, and control drums (Shemon et al., 2021). The top and bottom faces are set to insulated conditions, the coolant channel surface is set to a Dirichlet BC provided by THM, and the outer surface of the reflector exchanges heat by convection with the ambient environment at 30°C.

6.2. Multiphysics coupling

In this section, multiphysics coupling of THM, BISON, and OpenMC is performed for the full core geometry. Convergence was obtained in five Picard iterations; no instabilities were observed among the physics. Fig. 29 shows the fission power predicted by OpenMC; the BISON solid temperature is shown on a separate color scale in the non-fuel solid regions. In the axial direction, the power distribution is approximately sinusoidal, with a slight shift towards the core inlet where the fluid and solid temperatures are lower. Graphite temperatures are highest near the regions of

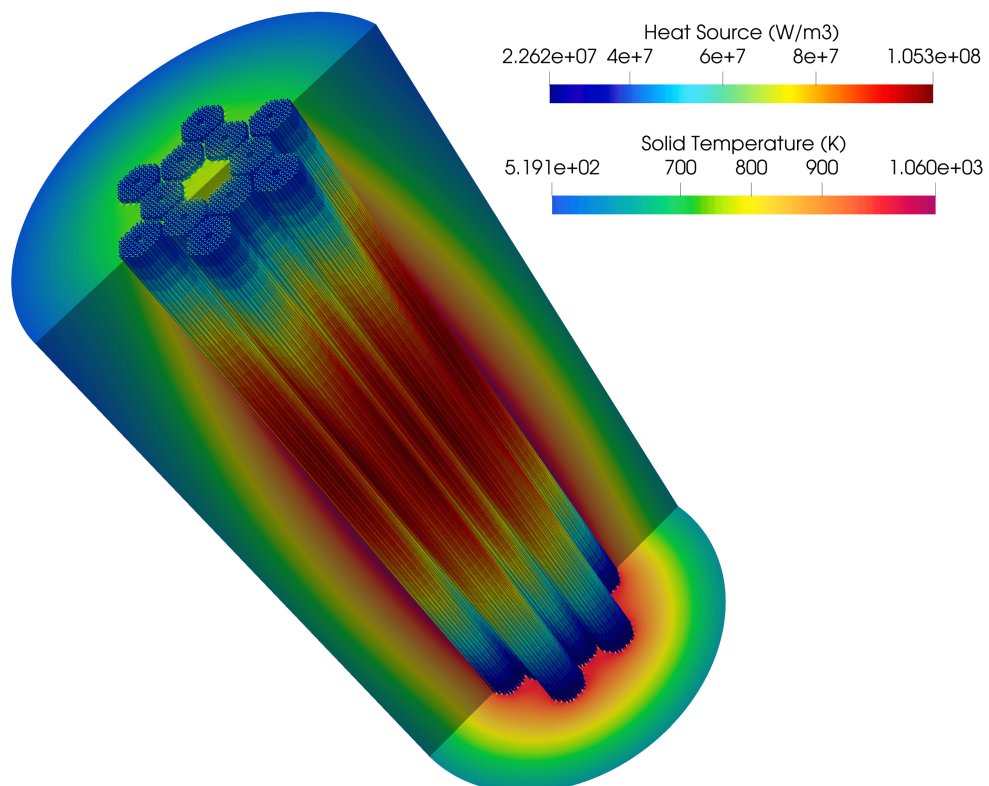


Fig. 29. OpenMC fission power in the fuel compacts, with the BISON solid temperature in the non-fuel regions (on a different color scale).

highest fission power, but shifted slightly downstream due to the combined effects of the power distribution and convective heat transfer.

Fig. 30 shows the OpenMC fission distribution on the core midplane. The poison compacts in the assembly corners induce a power depression in the adjacent fuel compacts. The power locally peaks near large quantities of graphite where moderation is strongest, especially near the core center. In terms of pin-averaged powers, the strong local variation in moderation results in a radial

power peaking factor of 1.57 on the core midplane. The highest powers are driven by the 36 fuel compacts closest to the core centerline (less than 0.5% of the total number of pins). This very strong local peaking in power will drive much higher fuel temperatures in these regions, but could be alleviated by modifying the burnable poison or fuel enrichment distributions.

Fig. 31 shows the BISON solid temperature in the core; heat is removed by helium coolant flowing in the downward direction through 1296 channels. Solid temperatures are highest near the core center where the power is highest. Convective heat removal at the outer radial boundary induces a large temperature drop over the radial reflector.

Fig. 32 shows the (a) BISON solid temperature and (b) OpenMC cell temperature through a zig-zag crosscut. The OpenMC cell temperatures are set as volume averages of all BISON mesh elements whose centroids map to that cell. These two figures are intentionally very similar to one another – looking closely in **Fig. 32(b)**, the cell divisions in the OpenMC model are visible. A similar temperature and density mapping is applied for the fluid regions. **Fig. 33** shows a zoomed-in view of **Fig. 32** to better illustrate the temperatures set in the OpenMC model in the fuel compacts.

As shown in **Fig. 32(a)**, fuel temperatures exceed the recommended long-term peak operating limits of TRISO fuels in the highest-powered compacts near the center of the core ([Demkowicz et al., 2019](#)). This is a combination of the preliminary reactor design as well as assumptions made in the computational model. Several sources of error are now briefly discussed.

By neglecting the interassembly helium gaps, the core graphite content is artificially increased by a small amount, on the order of 5%. This enhanced moderation is most significant near the assembly edges, which is also where the highest powers are observed. However, treating the interassembly gaps as stagnant helium only reduces powers by a few percent near the assembly peripheries.

Likely more significant in inducing high fuel temperatures is neglecting fluid flow in the interassembly gaps. The full core model assumed that all flow passed through the coolant channels, when in reality some percentage of the flow passes through gaps *between* assemblies. Predicting the percent of core flow that passes through the interassembly gaps (as opposed to through the coolant channels) is beyond the scope of the present work. Bypass fractions

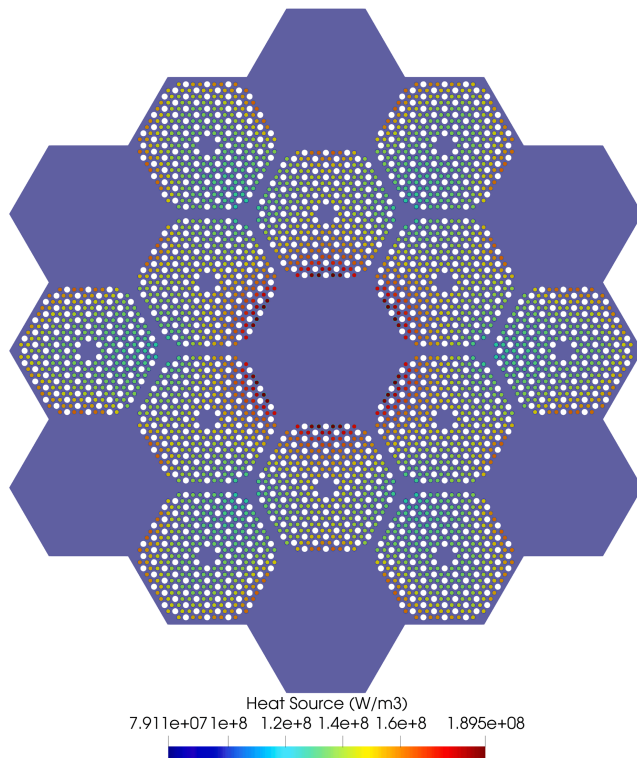


Fig. 30. OpenMC fission power distribution on the core midplane. Non-fuel regions are shown as a lilac color.

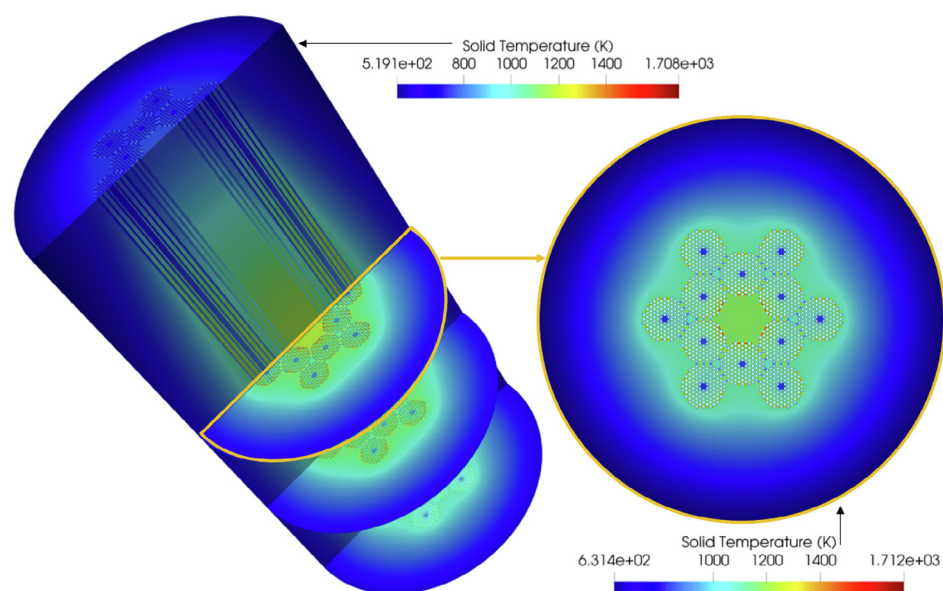
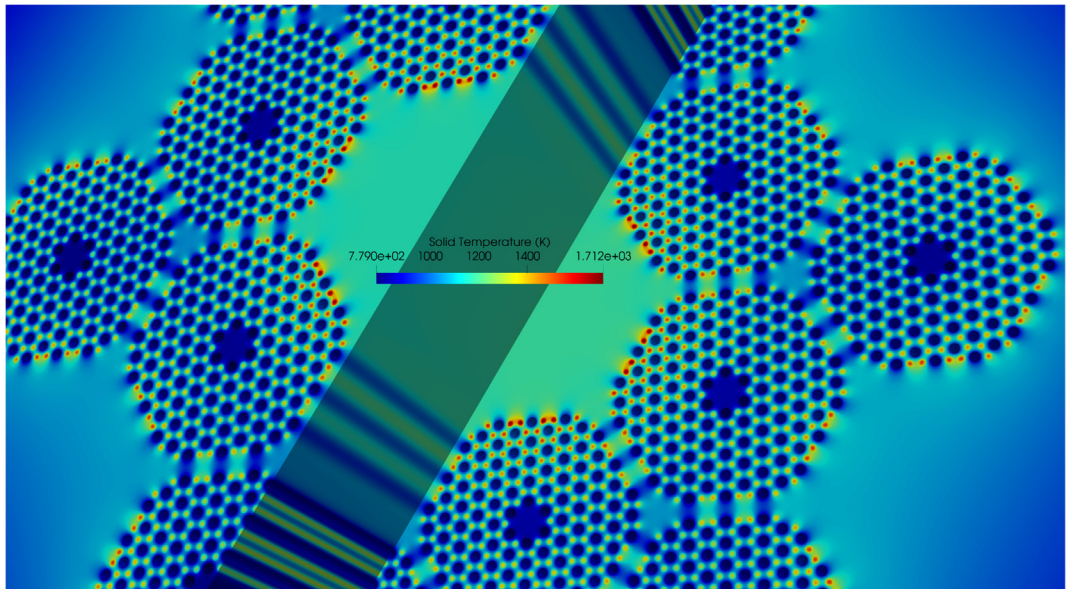
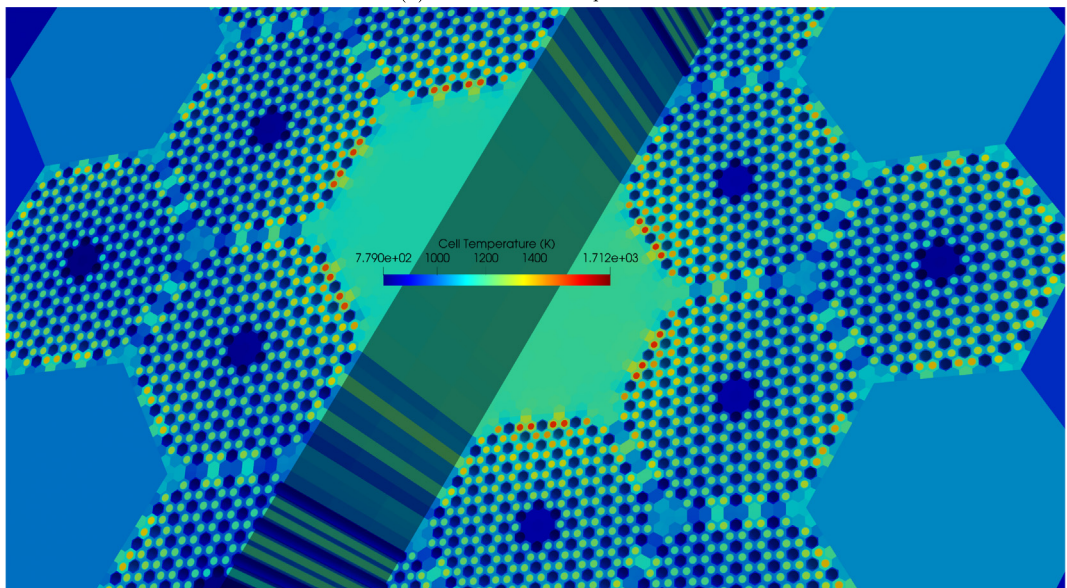


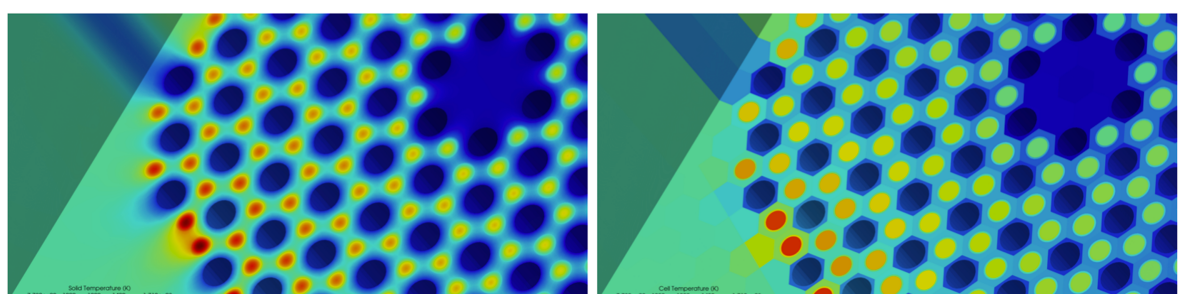
Fig. 31. BISON solid temperature. Note the use of different color scales for the left volume image and the right mid-plane view.



(a) BISON solid temperature



(b) OpenMC cell temperature

Fig. 32. Zoomed-in view of the (a) BISON solid temperature and (b) OpenMC cell temperature through a volume slice at $z = 2.79$ m and $z = 3.1715$ m from the core inlet.

(a) BISON solid temperature

(b) OpenMC cell temperature

Fig. 33. Zoomed-in view of the (a) BISON solid temperature and (b) OpenMC cell temperature at the bottom of the "step" shown in Fig. 32.

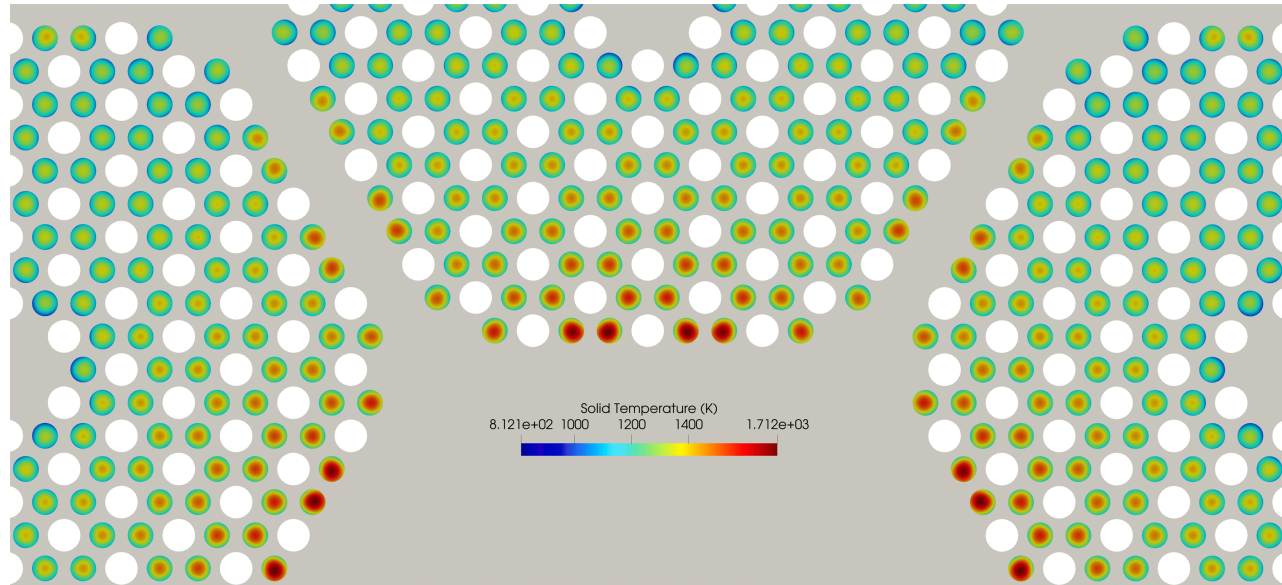


Fig. 34. Zoomed-in view of the BISON solid temperature in the fuel compacts along the core midplane.

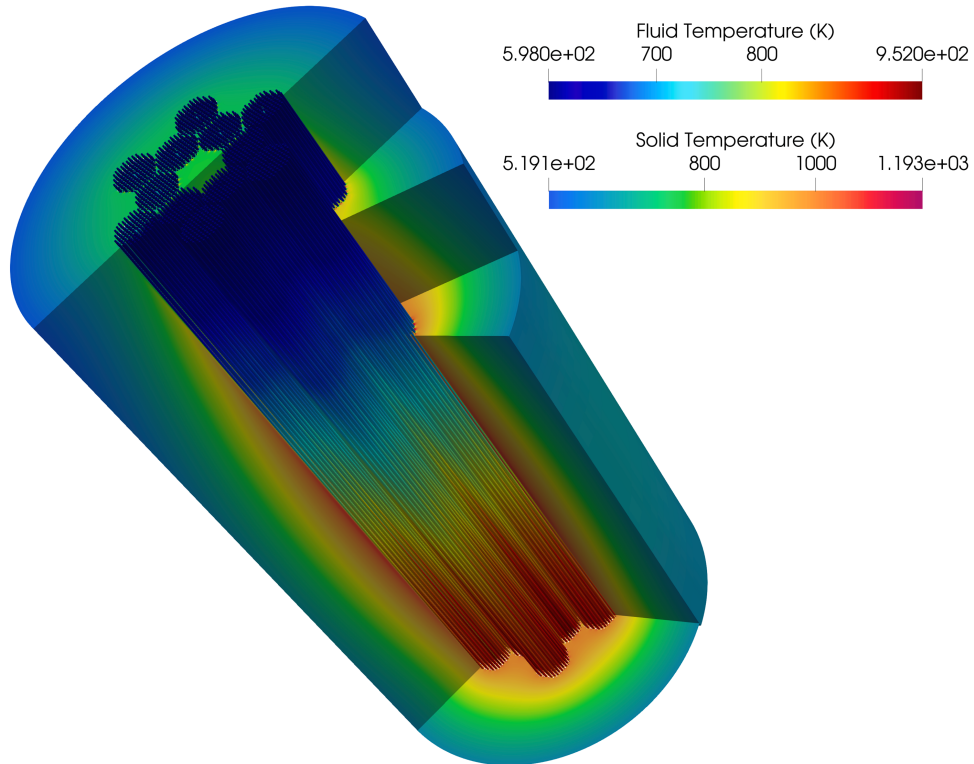


Fig. 35. THM fluid wall temperature in the coolant channels and BISON solid temperature in the non-fuel regions (on a different color scale).

through the graphite reflector blocks in pebble-type HTGRs are typically estimated to be on the order of 10% (Jun et al., 2013; Jun et al., 2011). Assuming some similarity to the graphite blocks in the present HTGR, a 10% bypass fraction would reduce the flow-rate through the coolant channels by 10%, but add a convective heat removal path in the interassembly spaces. Because the highest-temperature pins are adjacent to the assembly gaps, accounting for interassembly flow might reduce peak fuel temperatures by increasing the effective heat removal capacity for the edge pins (while only moderately decreasing the heat removal for fuel further removed from the assembly edges). Extensions of

the present model should account for interassembly flow to more accurately predict temperature distributions.

Fig. 34 shows the fuel temperature on the core midplane, zoomed into emphasize half of the assembly centered at $\theta = \pi/2$. The graphite monolith and the heterogeneous heat removal by coolant channels induce significant azimuthal temperature variations in the fuel compacts. Many fuel compacts exhibit surface temperature variations (maximum minus minimum surface temperatures) on the order of 200 K. Resolving 3-D heterogeneous solid heat conduction in prismatic HTGRs will be able to capture this azimuthal temperature variation.

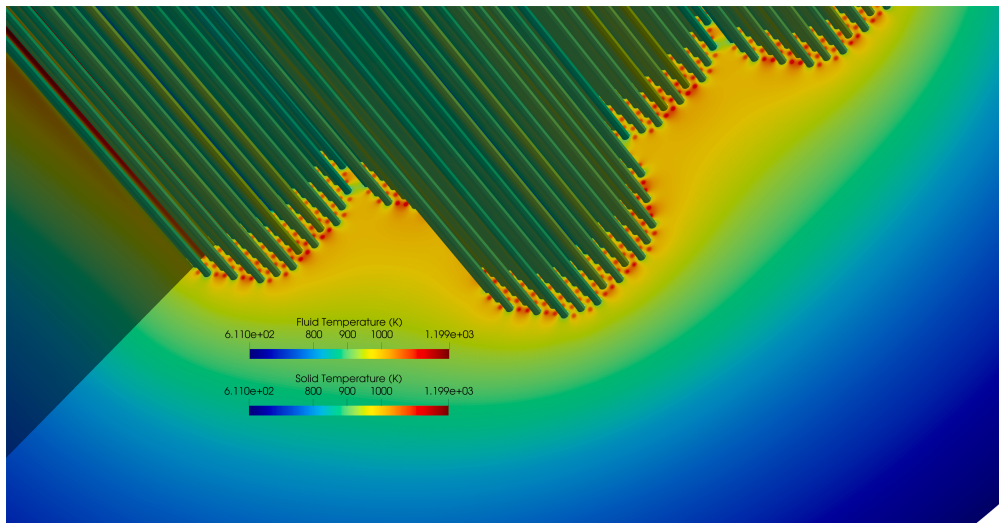


Fig. 36. THM fluid wall temperature in the coolant channels and BISON solid temperature in the solid regions.

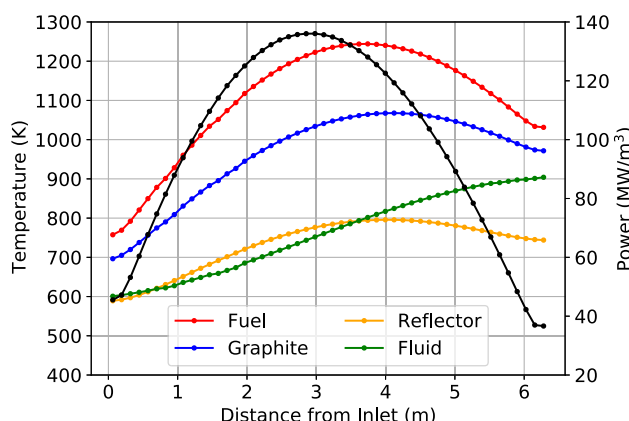


Fig. 37. Radially-averaged heat source and fuel, graphite, reflector, and fluid bulk temperatures.

Fig. 35 shows the THM fluid wall temperature in the coolant channels and the BISON solid temperature in the non-fuel regions (on a separate color scale). The fluid temperature continually increases moving through the core (from top to bottom) due to heat addition from the solid. Near the assembly corners where the poison compacts locally depress the power, less heat is removed by the adjacent coolant channels. These locally-reduced fluid temperatures are visible in Fig. 35.

Fig. 36 shows a zoomed-in view of Fig. 35, but with the BISON temperature shown in the fuel compacts as well as all non-fuel regions. The BC coupling on the coolant channel surface is visible by nature of the fluid-solid temperature continuity in these regions.

Finally, Fig. 37 shows the radially-averaged fuel, graphite, reflector, and fluid bulk temperatures as a function of height. The power distribution is shown in black, on the right axis. Here, “graphite” temperatures refers to the graphite monolith temperatures in the fuel assemblies and within several of the nearest adjacent graphite blocks (i.e., the light blue block IDs in Fig. 28). Due to the negative temperature coefficient, the power distribution peaks slightly upstream of the midplane. Neutron reflection within the upper and lower graphite reflectors is visible in the first nodes adjacent to these regions. All temperature distributions exhibit common trends observed in axial-flow systems; the fluid temperature rate of increase is highest near the midsection of the core,

where powers are highest. The fuel, graphite, and reflector temperatures all peak slightly downstream from the core midplane, due to the combined effects of the power distribution and the convective heat removal.

This concludes the full core modeling. This work has demonstrated that Cardinal can be used to resolve 3-D CHT and sub-pin power distributions in prismatic HTGRs. With future validation, Cardinal may be used for reactor design, providing reference solutions, and generating closures for lower-order tools.

A number of upcoming performance improvements to MOOSE and OpenMC will greatly improve computational performance and memory usage. Specifically, improvements to MOOSE’s MultiAppUserObjectTransfer are needed to allow the wall heat flux and temperature BCs between THM and BISON to leverage distributed mesh features. Currently, the full-core simulations require high-memory HPC nodes to fit all meshes in shared memory. The enhancement of the MultiAppUserObjectTransfer will allow the full-core simulations to distribute the BISON and THM meshes across MPI ranks, which will greatly reduce memory usage. In addition, a delta tracking implementation is nearing completion in OpenMC. For TRISO geometries with huge numbers of surface crossings in each particle track, we expect a factor of at least 2× speedup in the tracking rate. For simulations with BISON, OpenMC, and THM, over 90% of the total physics solve time is occupied by OpenMC (depending on the convergence tolerance for the tally uncertainty). Therefore, this upcoming delta tracking implementation will contribute significantly to reducing the total runtime. Future work will quantify typical computing requirements across a wide variety of applications.

7. Conclusions

Cardinal is an open-source MOOSE application (<https://github.com/neams-th-coe/cardinal>) that wraps NekRS spectral element CFD and OpenMC Monte Carlo radiation transport within the MOOSE framework, delivering high-resolution multiphysics feedback to diverse applications in nuclear engineering. As part of a NEAMS CoE project, this paper described a coupling of NekRS, OpenMC, BISON, and THM for multiphysics modeling of a prismatic HTGR. The applications shown in this work emphasized high-resolution multiphysics, multiscale closure generation, and the plug-and-play strengths of MOOSE’s MultiApp system.

Beginning with CHT modeling of a unit cell, a high-resolution coupling of NekRS–BISON was compared with a coarse-mesh coupling of THM–BISON. By comparing temperatures, it was shown that the 1-D area-averaged equations solved by THM are an excellent substitute for 3-D wall-resolved RANS for the coolant channels in prismatic block HTGRs. An important multiscale use case of NekRS was then demonstrated by generating a Nusselt number model for THM for the prototypic operating conditions. With a modest 8.5% correction to the Nusselt number, the THM and NekRS solid temperatures match with an average difference of only 4.7 K.

Next, multiphysics couplings of NekRS–BISON–OpenMC and THM–BISON–OpenMC were compared for an HTGR unit cell. The excellent thermal-fluid agreement between NekRS and THM causes the fission power predicted by NekRS–BISON–OpenMC and THM–BISON–OpenMC to match to within approximately 1%, which is on the order of statistical uncertainty in the tallies. This fine-scale comparison demonstrated that 1) THM is an appropriate substitute for NekRS for the thermal-fluid physics in the coolant channels in prismatic HTGRs, and 2) propagating small differences in the CHT physics to the neutron transport has negligible effect on the power distribution. Rigorous mesh refinement studies were performed for all physics, and a closer observation of the OpenMC model convergence illustrated the importance of resolving the low-power peripheral region in TRISO compacts.

Progressing from the unit cell, full-core simulations of the HTGR were conducted using THM, BISON, and OpenMC. Predictions were obtained for the fission distribution, solid temperatures, and fluid temperatures. The thermal-fluid physics predictions provide a clear motivation for 3-D heterogeneous CHT – fuel temperatures in each compact exhibited azimuthal asymmetries up to 200 K, with lower surface temperatures in areas facing the coolant channels. Significant moderation near the core centerline suggests that future models may improve accuracy by resolving flow in the inter-assembly gaps, which will preferentially cool peripheral fuel compacts with the strongest power peaking. These insights may also be used to guide burnable poison and fuel enrichment patterns in HTGRs.

While the computational model captured 3-D heat transfer and neutron transport in prismatic HTGRs, several key simplifications were assumed. Rather than explicitly mesh the TRISO particles in the BISON model, the heat source and material properties were homogenized into a single material. By distributing the thermal resistance of the low-conductivity buffer layer, this homogenization tends to underpredict peak fuel temperatures (Novak, 2020). Improved fidelity can be achieved by substituting in Pronghorn's multiscale TRISO models (Novak et al., 2021). In addition, flow in the interassembly regions was neglected by approximating the gaps as solid graphite, which may affect the azimuthal temperature variation in fuel compacts near assembly edges. In the OpenMC model, the axial reflectors were also neglected from the coupling, instead being set to the inlet or outlet temperatures. More accurate estimates of axial leakage may be obtained by incorporating reflector temperature feedback into the coupling.

Finally, there are a number of performance improvements on the near horizon. A delta tracking implementation is currently under development in OpenMC, which for TRISO systems is expected to improve the particle tracking rate. In addition, a steady passive scalar solver in NekRS has potential to significantly reduce the cost of NekRS simulations.

OpenMC has capabilities for Functional Expansion Tallies (FETs) (Ellis et al., 2017), and MOOSE contains native capabilities for transferring functional expansion coefficients between applications (Wendt et al., 2018). A near-term development activity will add an interface to OpenMC's FETs in Cardinal, enabling continuous representation of OpenMC's fission tally. For the full core geometry, each fuel compact was represented with 100 cell tallies. By

instead representing the power in each cylindrical HTGR fuel compact with Legendre and Zernike polynomials, a more highly-resolved power distribution can be obtained with far fewer tallies, translating to reduced cost to achieve the same statistical uncertainty. In addition, the automated convergence criteria that have been developed for FETs (Xiao et al., 2014) may simplify the tally independence studies required for multiphysics applications.

The main outcome of this work was a demonstration of Cardinal's capabilities for prismatic HTGRs. By using physics- and geometry-agnostic couplings to MOOSE, Cardinal may have a transformative impact on the inclusion of high-resolution multiphysics feedback in diverse nuclear engineering applications.

CRediT authorship contribution statement

A.J. Novak: Conceptualization, Methodology, Software, Validation, Investigation, Writing – original draft, Visualization, Project administration. **D. Andrs:** Methodology. **P. Shriwise:** Methodology, Software. **J. Fang:** Methodology. **H. Yuan:** Methodology. **D. Shaver:** Supervision, Project administration. **E. Merzari:** Conceptualization, Validation. **P.K. Romano:** Resources, Writing - review & editing. **R. C. Martineau:** Conceptualization, Resources, Writing - review & editing, Funding acquisition.

Declaration of Competing Interest

The authors declare that they have no known competing financial interests or personal relationships that could have appeared to influence the work reported in this paper.

Acknowledgements

This material is based upon work supported by Laboratory Directed Research and Development (LDRD) funding from Argonne National Laboratory (ANL), provided by the Director, Office of Science, of the U.S. DOE under Contract No. DE-AC02-06CH11357. ANL's work was also supported by the U.S. Department of Energy, Office of Nuclear Energy, NEAMS program, under contract DE-AC02-06CH11357.

We gratefully acknowledge the computing resources provided on Bebop, a high-performance computing cluster operated by the Laboratory Computing Resource Center at ANL.

References

- Demkowicz, P.A., Liu, B., Hunn, J.D., 2019. Coated Particle Fuel: Historical Perspectives and Current Progress. *J. Nucl. Mater.* 515, 434–450.
- McDonald, C.F., 1990. Gas Turbine Power Plant Possibilities with a Nuclear Heat Source: Closed and Open Cycles. *Gas Turbine and Aeroengine Congress and Exposition*.
- Graham, L.W., 1990. Corrosion of Metallic Materials in HTR-Helium Environments. *J. Nucl. Mater.* 171, 76–83.
- Zheng, G., Sridharan, K., 2018. Corrosion of Structural Alloys in High-Temperature Molten Fluoride Salts for Applications in Molten Salt Reactors. *JOM* 70, 1535–1541.
- Ma, Y., Liu, M., Xie, B., Han, W., Yu, H., Huang, S., Chai, X., Liu, Y., Zhang, Z., 2021. Neutronic and Thermal-Mechanical Coupling Analyses in a Solid-State Reactor Using Monte Carlo and Finite Element Methods. *Ann. Nucl. Energy* 151, 107923.
- Novak, A.J., Andrs, D., Shriwise, P., Shaver, D., Romano, P.K., Merzari, E., Keutelian, P., 2022. Coupled Monte Carlo Transport and Thermal-Hydraulics Modeling of a Prismatic Gas Reactor Fuel Assembly Using Cardinal. *Proceedings of Physor*.
- V.M. Laboure, J. Ortenzi, Y. Wang, S. Schunert, F.N. Gleicher, M.D. DeHart, R.C. Martineau. Multiphysics Steady-State Simulation of the High Temperature Test Reactor with MAMMOTH, BISON and RELAP-7. Technical Report INL/CON-18-52202-Revision-0, Idaho National Laboratory, 2019.
- P. Fischer, S. Kerkemeier, M. Min, Y. Lan, M. Phillips, T. Rathnayake, E. Merzari, A. Tomboulides, A. Karakus, N. Chalmers, and T. Warburton. NekRS, a GPU-Accelerated Spectral Element Navier-Stokes Solver, April 2021. arXiv:2104.05829.
- Romano, P.K., Horelik, N.E., Herman, B.R., Nelson, A.G., Forget, B., Smith, K., 2015. OpenMC: A State-of-the-Art Monte Carlo Code for Research and Development. *Ann. Nucl. Energy* 82, 90–97.

- Permann, C.J., Gaston, D.R., Andrš, D., Carlsen, R.W., Kong, F., Lindsay, A.D., Miller, J.M., Peterson, J.W., Slaughter, A.E., Stogner, R.H., Martineau, R.C., 2020. MOOSE: Enabling massively parallel multiphysics simulation. Software 11, 100430.
- Novak, A.J., Shriwise, P., Rahaman, R., Romano, P.K., Merzari, E., Gaston, D., 2022. Coupled Monte Carlo Transport and Conjugate Heat Transfer for Wire-Wrapped Bundles Within the MOOSE Framework. Proceedings of Nureth.
- Merzari, E., Yuan, H., Min, M., Shaver, D., Rahaman, R., Shriwise, P., Romano, P., Talamo, A., Lan, Y., Gaston, D., Martineau, R., Fischer, P., Hassan, Y., 2021. Cardinal: A Lower Length-Scale Multiphysics Simulator for Pebble-Bed Reactors. Nucl. Technol.
- P. Fischer, E. Merzari, M. Min, S. Kerkemeier, Y. Lan, M. Phillips, T. Rathnayake, A. Novak, D. Gaston, N. Chalmers, and T. Warburton. Highly Optimized Full-Core Reactor Simulations on Summit, October 2021. arXiv:2110.01716.
- Huxford, A., Petrov, V., Manera, A., Coppo Leite, V., Merzari, E., Zou, L., 2022. Development of Innovative Overlapping-Domain Coupling Between SAM and nekRS. In: Proceedings of NURETH.
- Yu, Y., Novak, A., Shaver, D., Merzari, E., 2022. Coupled Simulation of Reactor Pressure Vessel (RPV) Subjected to Pressurized Thermal Shock (PTS) Using Cardinal. In: Proceedings of ATH.
- R.A. Berry, J.W. Peterson, H. Zhang, R.C. Martineau, H. Zhao, L. Zou, and D. Andrš. RELAP-7 Theory Manual. Technical Report INL/EXT-14-31366, Idaho National Laboratory, 2014
- J.D. Hales, R.L. Williamson, S.R. Novascone, G. Pastore, B.W. Spencer, D.S. Stafford, K. A. Gamble, D.M. Perez, R.J. Gardner, W. Liu, J. Galloway, C. Matthews, C. Unal, and N. Carlson. BISON Theory Manual. Technical Report INL/EXT-13-29930 Rev. 3, Idaho National Laboratory, 2016.
- Cardinal: An Open-Source Coupling of NekRS and OpenMC to MOOSE. URL: <https://cardinal.cels.anl.gov>, 2022.
- Feng, B., Fang, J., Hua, T., Stauf, N., Novak, A., Zou, L., Hu, R., Balestra, P., Reger, D., Martin, N., Giudicelli, G., Abou-Jaoude, A., 2021. Single- and Multi-Physics Models of Advanced Reactors in the Virtual Test Bed. In: Proceedings of ANS.
- Trumbull, T.H., 2006. Treatment of Nuclear Data for Transport Problems Containing Detailed Temperature Distributions. Nucl. Technol. 156, 75–86.
- Seker, V., Thomas, J., Downar, T., 2007. Reactor Simulation with Coupled Monte Carlo and Computational Fluid Dynamics. In: Proceedings of Joint International Topical Meeting on Mathematics and Computation and Supercomputing in Nuclear Applications.
- Vazquez, M., Tsige-Tamirat, H., Ammirabile, L., Martin-Fuertes, F., 2012. Coupled Neutronics Thermal-Hydraulics Analysis Using Monte Carlo and Sub-Channel Codes. Nucl. Eng. Des. 250, 403–411.
- A. Ivanov, V. Sanchez, U. Imke, Development of a Coupling Scheme Between MCNP5 and SUBCHANFLOW for the Pin- and Fuel Assembly-Wise Simulation of LWR and Innovative Reactors. In Proceedings of M & C, 2011.
- J.C. Kok, S.P. Spekreijse. Efficient and Accurate Implementation of the $k-\omega$ Turbulence Model in the NLR Multi-Block Navier-Stokes System. In European Congress on Computational Methods in Applied Sciences and Engineering, 2000.
- S. Thangam, R. Abid, C.G. Speziale, Application of a New $k-\tau$ Model to Near Wall Turbulent Flows. Technical Report AD-A232 844 No. 91-16, NASA Langley Research Center, 1991.
- A. Fichtner. Full Seismic Waveform Modelling and Inversion. Springer, 2011.
- Churchill, S.W., 1977. Friction-Factor Equation Spans All Fluid-Flow Regimes. Chem. Eng. 84, 91–92.
- Kamalpour, S., Salehi, A.A., Khalafi, H., Mataji-Kojouri, N., Jahanfarnia, G., 2018. The Potential Impact of Fully Ceramic Microencapsulated (FCM) Fuel on Thermal Hydraulic Performance of SMART Reactor. Nucl. Eng. Des. 339, 39–52.
- Zhang, C., Wu, Y., He, Y., Li, Y., Liu, S., Zhang, J., Tian, W., Su, G.H., Qiu, S., Wu, J., 2021. Investigation on Thermo-Mechanical Performance of Full Ceramic Microencapsulated Fuel. J. Nucl. Mater. 556, 153171.
- Weng, M., Liu, S., Liu, Z., Qi, F., Zhou, Y., Chen, Y., 2021. Development and Application of Monte Carlo and COMSOL Coupling Code for Neutronics-Thermohydraulics Coupled Analysis. Ann. Nucl. Energy 161, 108459.
- Novak, A.J., Schunert, S., Carlsen, R.W., Balestra, P., Slaybaugh, R.N., Martineau, R.C., 2021. Multiscale Thermal-Hydraulic Modeling of the Pebble Bed Fluoride-Salt-Cooled High-Temperature Reactor. Ann. Nucl. Energy 154, 107968.
- A.J. Novak. Multiscale Thermal-Hydraulic Methods for Pebble Bed Reactors. PhD thesis, University of California, Berkeley, 2020.
- Novak, A.J., Carlsen, R.W., Schunert, S., Balestra, P., Reger, D., Slaybaugh, R.N., Martineau, R.C., 2021. Pronghorn: A Multidimensional Coarse-Mesh Application for Advanced Reactor Thermal Hydraulics. Nucl. Technol. 207, 1015–1046.
- Stainsby, R., Grief, A., Worsley, M., Dawson, F., 2009. Investigation of Local Heat Transfer Phenomena in a Pebble Bed HTGR Core. Technical report, AMEC Nuclear.
- A.J. Novak, S. Schunert, R.W. Carlsen, P. Balestra, D. Andrš, J. Kelly, R.N. Slaybaugh, R. C. Martineau, Pronghorn Theory Manual. Technical Report INL/EXT-18-44453-Rev001, Idaho National Laboratory, 2020.
- R. Hu, SAM theory manual. Technical Report ANL/NE-17/4, Argonne National Laboratory, 2017.
- Ivanov, A., Sanchez, V., Stieglitz, R., Ivanov, K., 2013. High Fidelity Simulation of Conventional and Innovative LWR with the Coupled Monte-Carlo Thermal-Hydraulic System MCNP5-SUBCHANFLOW. Nucl. Eng. Des. 262, 264–275.
- Zhang, Q., Peng, T., Zhang, G., Liu, J., Guo, X., Gong, C., Yang, B., Fan, X., 2021. An Efficient Scheme for Coupling OpenMC and FLUENT With Adaptive Load Balancing. Sci. Technol. Nucl. Install. 2021, 5549602.
- Mylonakis, A.G., Varvayanni, M., Catsaros, N., 2017. A Newton-Based Jacobian-Free Approach for Neutronic-Monte Carlo/Thermal-Hydraulic Static Coupled Analysis. Ann. Nucl. Energy 110, 709–725.
- Guo, J., Liu, S., Shen, Q., Huang, S., Wang, K., 2017. A Versatile Method of Coupled Neutronics/Thermal-Hydraulics Based on HDF5. In: Proceedings of M&C.
- Gurecky, W., Schneider, E., 2016. Development of an MCNP6-ANSYS FLUENT Multiphysics Coupling Capability. In: Proceedings of ICONE.
- Romano, P., Hamilton, S., Rahaman, R., Novak, A., Merzari, E., Harper, S., Shriwise, P., 2020. Design of a Code-Agnostic Driver Application for High-Fidelity Neutronic and Thermal-Hydraulic Simulations. In: Proceedings of PHYSOR.
- Liu, S., Liang, J., Wu, Q., Guo, J., Huang, S., Tang, X., Li, Z., Wang, K., 2017. BEAVRS Full Core Burnup Calculation in Hot Full Power Condition by RMC Code. Ann. Nucl. Energy 101, 434–446.
- Xexin, O., Huang, S., Liu, S., Wang, K., 2017. Internal Coupling Scheme in RMC with Thermal-Hydraulics Feedback and On-the-fly Doppler Broadening Method. In: Proceedings of M&C.
- Dufek, J., Gudowski, W., 2006. Stochastic Approximation for Monte Carlo Calculation of Steady-State Conditions in Thermal Reactors. Nucl. Sci. Eng. 152, 274–283.
- Shen, Q., Boyd, W., Forget, B., Smith, K., 2015. Tally Precision Triggers for the OpenMC Monte Carlo Code. In: Trans. Am. Nucl. Soc.
- J.W. Sterbentz, P.D. Bayless, L.O. Nelson, H.D. Gougar, J.C. Kinsey, G. Strydom, and A. Kumar. High-Temperature Gas-Cooled Test Reactor Point Design. Technical Report INL/EXT-16-38296, Idaho National Laboratory, 2016.
- M. Fratoni. Development and Applications of Methodologies for the Neutronic Design of the Pebble Bed Advanced High Temperature Reactor (PB-AHTR). PhD thesis, University of California, Berkeley, 2008.
- Brown, F.B., 2006. On the Use of Shannon Entropy of the Fission Distribution for Assessing Convergence of Monte Carlo Criticality Calculations. In: Proceedings of PHYSOR.
- Incropera, F.P., Dewitt, D.P., 2011. Fundamentals of Heat and Mass Transfer. John Wiley & Sons.
- R.H.S. Winterton. Where did the Dittus and Boelter Equation Come From. Int. J. Heat Mass Transfer, 41:809–810, 1998.
- Ferraro, D., Garci, M., Imke, U., Valtavirta, V., Leppanen, J., Sanchez-Espinoza, V., 2019. Serpent/SCF Pin-Level Multiphysics Solutions for the VERA Fuel Assembly Benchmark. Ann. Nucl. Energy 128, 102–114.
- Suikkanen, H., Rintala, V., Schubert, A., Uffelen, P.V., 2020. Development of Coupled Neutronics and Fuel Performance Analysis Capabilities between Serpent and TRANSURANUS. Nucl. Eng. Des. 359, 110450.
- Shemon, E., Mo, K., Miao, Y., Jung, Y., Richards, S., Oaks, A., Kumar, S., 2021. MOOSE Framework Enhancements for Meshing Reactor Geometries. Proceedings of Physor.
- Jun, S., Yanhua, Z., Fu, L., 2013. Various Bypass Flow Paths and Bypass Flow Ratios in HTR-PM. Energy Procedia 39, 258–266.
- Jun, S., Yanhua, Z., Fu, L., 2011. Researches of Bypass Flows from Cold Plenum to Hot Plenum in HTR-PM by the Flow Network Method. In: Proceedings of Icone.
- Ellis, M., Gaston, D., Forget, B., Smith, K., 2017. Preliminary Coupling of the Monte Carlo Code OpenMC and the Multiphysics Object-Oriented Simulation Environment for Analyzing Doppler Feedback in Monte Carlo Simulations. Nucl. Sci. Eng. 185, 184–193.
- Wendt, B., Novak, A.J., Romano, P., Kerby, L., 2018. Integration of Functional Expansion Methodologies as a MOOSE Module. In: Proceedings of PHYSOR.
- Xiao, Y., Hu, L., Qiu, S., Zhang, D., Su, G., Tian, W., 2014. Development of a Thermal-Hydraulic Analysis Code and Transient Analysis for a FHTR. In: Proceedings of the International Conference on Nuclear Engineering.